Review Article

Mohammed Ali Dheyab*, Jia Hui Tang, Azlan Abdul Aziz*, Shaymaa Hussein Nowfal, Mahmood S. Jameel, Mohammad Alrosan, Nazila Oladzadabbasabadi and Mehran Ghasemlou*

Green synthesis of gold nanoparticles and their emerging applications in cancer imaging and therapy: a review

https://doi.org/10.1515/revic-2024-0048
Received June 30, 2024; accepted November 8, 2024;
published online November 29, 2024

Abstract: The green and eco-friendly synthesis of gold nanoparticles (AuNPs) from renewable resources such as plants, algae, fungi, and bacteria has recently gained interest due to its use of sustainable feedstocks. This review presents an in-depth exploration of AuNP synthesis methods and their applications in cancer imaging and therapy. We examine the mechanisms behind various physical and chemical techniques used to synthesize AuNPs, with a special focus on the unique biomedical applications of green-synthesized AuNPs in diagnostic and therapeutic platforms, such as imaging and targeted therapy. Although promising, green synthesis of AuNPs faces challenges, including variability in particle size, limitations in morphology control, and scalability issues, which need to be addressed to fully harness their potential. This review also demonstrates that AuNPs can be loaded with anti-cancer agents to create targeted drug delivery vehicles for tumor treatment. As nanotechnology drives revolutionary advances in healthcare, AuNPs offer a promising toolkit for medical progress. However, a fundamental understanding of AuNPs and rigorous risk assessments in diagnostics, imaging, and therapeutic applications are essential to enable their safe and effective use in clinical settings.

Keywords: AuNPs; green synthesis; cancer imaging; diagnostic; cancer therapy

***Corresponding authors: Mohammed Ali Dheyab and Azlan Abdul Aziz**, School of Physics, Universiti Sains Malaysia, 11800, Pulau Pinang, Malaysia; and Nano-Biotechnology Research and Innovation (NanoBRI), Institute for Research in Molecular Medicine (INFORMM), Universiti Sains Malaysia, 11800, Pulau Pinang, Malaysia, E-mail: mdali@usm.my (M. Ali Dheyab), lan@usm.my (A. Abdul Aziz). https://orcid.org/0000-0003-0585-7858 (M. Ali Dheyab); and **Mehran Ghasemlou**, School of Science, STEM College, RMIT University, Melbourne, VIC 3001, Australia; and Centre for Sustainable Bioproducts, Deakin University, Waurn Ponds, VIC 3216, Australia, E-mail: m.ghasemlou@deakin.edu.au
Jia Hui Tang, School of Physics, Universiti Sains Malaysia, 11800, Pulau Pinang, Malaysia. https://orcid.org/0009-0008-7736-3228
Shaymaa Hussein Nowfal, Medical Physics Department, College of Science, University of Warith Al-Anbiyaa, Karbala, Iraq; and Medical Physics Department, College of Applied Medical Sciences, University of Kerbala, Karbala, Iraq
Mahmood S. Jameel, Pharmaceutical Design and Simulation Laboratory, School of Pharmaceutical Sciences, Universiti Sains Malaysia, 11800, Pulau Pinang, Malaysia
Mohammad Alrosan, Applied Science Research Center, Applied Science Private University, Al-Arab St. 21, Amman 11931, Jordan
Nazila Oladzadabbasabadi, School of Science, STEM College, RMIT University, Melbourne, VIC 3001, Australia

1 Introduction

Nanotechnology is an emerging technology that allows the manipulation of matter with sizes ranging from 1 to 100 nm, regardless of shape.[1–6] Nanotechnology is a rapidly evolving field, giving birth to countless subfields either by creating new nanoscale materials or increasing the performance of already-existed microscale materials.[7] It is perhaps unsurprising the first appearance of inorganic nanoparticles (NPs) occurred in the Greco-Roman period.[8] Since then, the fast growth of nanotechnology advancement and material nanoscale engineering, enabled the widespread development of different types of NPs in almost every industry. Controlling the size of NPs, which often falls at the intermediate of atom and molecule, is critically important in clinical settings to treat incurable diseases.[7,9]

Amongst NPs, the synthesis of gold nanoparticles (AuNPs) has been largely documented.[10–12] Gold (Au) is known as a chemically inert metal and is widely considered benign to the human body. With the rise of nanotechnology and the discovery of new nanomaterials, the study of Au's physical and chemical properties has seen a progressive advancement in many fields, particularly the biomedical industry.[13,14] This surge of interest stemmed from several

unique merits of AuNPs, such as biocompatibility, non-toxicity to human tissues, tumor-targeting ability, ease of functionalization, and light-interacting ability to interact with light and more.[7,15,16] Most metallic NPs are not fully biocompatible and, hence, may not be useful for medical applications. A unique advantage of AuNPs that distinguishes them from other metallic NPs is their minimal-to-non toxicity and chemically inert character.[17] These benefits allow them to compete with conventional medical treatments for anticancer therapies and diagnostic imaging.[18] The immense potential of AuNPs as a relatively new technology in clinical settings has begun to be recognized, and the research investment to synthesize them using green and/or sustainable feedstocks has enormously increased globally.[19] Recent studies have demonstrated the successful integration of AuNPs in clinical applications, notably in diagnostic imaging,[20] targeted drug delivery,[21] and as radiosensitizers in cancer therapies.[22] AuNPs have been explored as contrast agents in computed tomography (CT)[23] and photoacoustic imaging,[24] showing better resolution and localization of cancerous tissues than traditional contrast agents. In oncology, AuNPs have shown potential in enhancing the effectiveness of radiation therapy through targeted radiosensitization, which minimizes harm to surrounding healthy tissues.[25] These advancements underscore the clinical significance of AuNPs and motivate ongoing research into green synthesis methods that maximize biocompatibility and therapeutic efficacy while reducing environmental impact.

There are different techniques available for synthesizing AuNPs. These are generally categorized into top–down and bottom–up methods. The top–down synthesis method is the process of physically breaking down bulk materials to produce nano-sized NPs, while in the bottom–up synthesis method, atomic-sized materials are assembled to form the NPs.[7,26] Top–down approaches are frequently referred to as physical and chemical methods, while bottom–up approaches are often termed as chemical methods.[27] Spray pyrolysis and laser ablation are two common top–down methods to synthesize AuNPs. Top–down approaches are most widely used for synthesizing AuNPs due to their simplicity, usage of toxic-free chemicals, and favorable properties of products such as purity, uniformity, shape, and size.[28,29] Chemical methods to synthesize AuNPs have occupied the mainstream of recent publications due to their lower cost and energy consumption compared to physical methods.

Although chemical methods seem to synthesize AuNPs much more easily, they have major drawbacks. The major bottleneck associated with chemical methods is the presence of toxicity of the solvents used as reducing agents. The non-environmental friendliness of chemical methods has led to the development of green and solvent-free technologies without damaging the environment.[30] The green synthesis of AuNPs using living organisms such as microorganisms, mushrooms, plants, and other agricultural waste, which follows the bottom–up strategy, is an alternative route to substitute the chemical methods.[31–33] Unlike physical methods, green biosynthesis of AuNPs is straightforward, affordable, ecologically friendly, and easy to scale up; these merits are sufficient to obtain large-scale commercial yields.[31] Hence, given the ongoing environmental concerns, using green reducing agents has now evolved into a single strategy to synthesize AuNPs on commercial levels.[34] The existence of bio-compounds in microbial organisms, such as enzymes, sugars, aldehydes, and proteins, could endow positive effects on the growth and formation of AuNPs.[35,36] Remarkably, these bio-compounds not only contribute to the reduction process but also act as capping agents to stabilize the AuNPs.[37] Recently, our group reviewed the use of AuNPs-based photothermal therapy (PTT) for breast cancer cells, summarizing the various sizes and characteristics of different AuNP types.[38] In another study, we focused on monodisperse AuNPs synthesized via various methods for diverse diagnostic and therapeutic applications.[39] Alizadeh et al. discussed applications involving AuNP aggregation,[40] while Mitri et al. reviewed and compared data from studies published between 2015 and 2022, highlighting key biological compounds and outcomes from *in vitro* and *in vivo* applications of green or biosynthesized AuNPs.[41] Despite these reports, further studies are needed to understand, compare and contrast conventional chemical synthesis methods of AuNPs with alternative green synthesis methods, emphasizing the unexpectedly improved properties discovered through green synthesis approaches.

This review article constitutes a substantial advancement in the field by providing an extensive and current overview of the potential applications of AuNPs synthesis from bacteria, plants, and algae in various medical domains such as anticancer and antibacterial treatments and examines their future directions in cancer therapy and diagnosis. It not only assesses recent studies but also delineates the limitations and challenges associated with utilizing green-synthesized AuNPs in medical contexts. Furthermore, the article explores traditional green synthesis techniques, recent breakthroughs, and innovative approaches for AuNP synthesis, elucidating their respective merits, drawbacks, and prospective medical uses, thereby paving the way for future research endeavors in the field.

2 Production and synthesis of AuNPs

2.1 Physical methods

The ultrasonic spray pyrolysis (USP) technique is one of the common physical methods that has gained strong potential for large-scale production of AuNPs.[42] The synthesis of AuNPs using USP is straightforward and versatile, and the functional properties of the NPs can be tuned by changing the process parameters.[43] Because of operating at ambient conditions (i.e., room temperature and atmospheric pressure), which consumes less energy, USP is considered more affordable than other physical processes such as ball milling, ultrasonic machining, laser ablation.[44] A USP device is composed of an ultrasonic generator, a reaction chamber, and a collection medium, which typically serve as a stabilizing agent to prevent/minimize agglomeration.[42,45] For running a USP process, the droplets of Au precursor solution are first generated by the ultrasonic generator. These droplet-like aerosol particles are then passed into the heating chamber using an inert carrier gas. After the complete chemical reactions at extremely high temperatures, the droplets containing AuNPs are then collected[42] (Figure 1). Bekić at el.[46] reported the synthesis of AuNPs through the USP technique using hydrogen tetrachloroaurate (III) hydrate ($HAuCl_4{\cdot}3H_2O$) as the precursor. The precursor was first subjected to an ultrasonic aerosol generator at a frequency of 2.5 MHz to form aerosol droplets of the solution. A nitrogen carrier gas at the flow range of 1–4.5 L/min then transported the aerosol droplets to the heating zones via a quartz tube. To generate pure AuNPs, hydrogen gas (H_2) was added as the reducing agent to the flowing nitrogen gas. At the first heating zone (referred to as evaporation zone), the temperature was set in the range of 50–100 °C to evaporate and dry the aerosol particles. At the second heating zone, the drying temperature increased to 260–500 °C to enable the formation of AuNPs. After completing the reaction, the AuNPs were collected in a separate collection medium containing sodium citrate solution as a stabilizer. The observation of AuNPs particles using high-resolution TEM and SEM revealed an approximate size of 20 nm and spherical or polyhedron shapes. A characterization using UV–vis spectroscopy, the surface plasmon resonance (SPR) peak was found to be located at the wavelength of 530 nm, the conclusion drawn from the wavelength shift from 530 nm to 532 nm after coating AuNPs with PVP and PEG suggests that the increase in hydrodynamic size and the shift in the SPR peak is likely attributed to the coating of AuNPs with larger polymers, PVP and PEG. This conclusion indicates that the coating process alters the optical properties of the AuNPs, affecting their interaction with light. Similarly, Golub et al.[42] dissolved $HAuCl_4$ salt in deionized water and magnetically stirred the mixture until its color turned a bright yellow. This yellowish solution was used as the precursor for the synthesis of AuNPs. The authors then used an ultrasonic nebulizer, which was operated at a frequency of 2.5 MHz to generate submicron aerosol droplets. The aerosols were then transferred to the heating zones via a quartz glass tube using nitrogen as the carrier gas (6 L/min). Hydrogen gas (3 L/min) was mixed with the gas inlet for the reduction of the aerosol droplets to AuNPs. The heating region was designed to have four different zones: one evaporation zone, which separates the aerosol droplets, and three drying zones, which dry the particles. The temperature in the evaporation zone was 120 °C, while the temperature in three consecutive reaction zones was 350 °C to allow the synthesis of AuNPs. The polyvinylpyrrolidone (PVP)-coated AuNPs

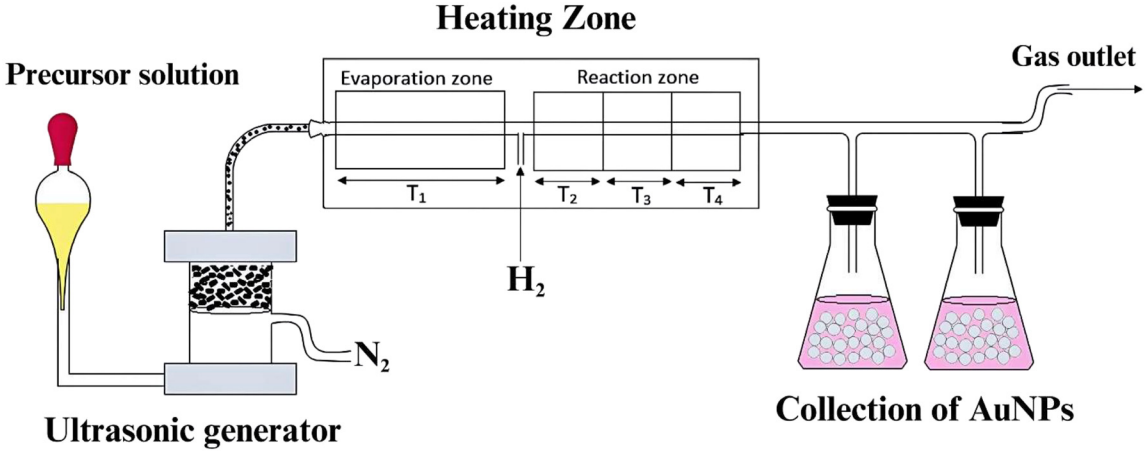

Figure 1: A schematic presentation of an ultrasonic spray pyrolysis (USP) technique that is composed of an ultrasonic nebulizer, a four-zone heating region, collection bottles, a gas inlet and outlet, and a quartz transport tube. Adapted from ref. 42.

with a nominal size of 28.04 nm were then collected in a collection medium. The colloidal AuNPs remained stable with the presence of SPR at 532 nm.

Laser ablation (LA) is another physical method that removes NPs from a target metal surface. During laser ablation, a high-energy pulsed laser beam is irradiated on top of the metal solid surface. Ablation (vaporization and ejection of fragments) only occurs when the metal surface absorbs sufficient energy.[47] Laser ablation in liquid (LAL) has been investigated by many groups to enhance the efficiency of the laser greatly. Figure 2a depicts a schematic illustration of a typical LAL system that is often used for synthesizing AuNPs. The ablation of a bulk material immersed in a liquid prevents the re-deposition of ablated NPs on the material's surface. The liquid environment also absorbs the heat of the metal target, preventing excessive heat build-up.[31] Shamari et al.[48] devised an ablation apparatus that used highly pure Au targets in their experiment. Before ablation, the target was sanded and sonicated in an organic solvent. The Au was then washed with chlorobenzene and distilled water several times to eliminate any possible impurities on the surface. The ablation was performed using a high-energy Nd:YAG laser that operated at a pulse frequency of 10 Hz, an emission wavelength of 1,064 nm, a width pulse of 6 nm, and a laser power of 4 W. A convex lens (focal length = 10 cm) was used to guide the laser beam to focus perpendicularly onto the target surface. The Au target was submerged in water before being irradiated with a laser beam. The X-ray diffraction (XRD) and UV–vis spectroscopy results collectively validated the production of crystalline AuNPs with the face-centered cubic crystal structure. The TEM imaging revealed the average diameter of the spherical AuNPs to be around 10–25 nm. In another study, Menazea et al.[49] obtained AuNPs with a diameter of 20 nm through an ablation process that lasted only 10 min. The authors used an Au plate with 99.99 % purity, which had been polished repeatedly using ultra-fine emery paper, followed by washing in water. The process used a mixture of chitosan (CS) and polyvinyl alcohol (PVA) in a ratio of 7:3 ratio as the liquid medium. An Nd:YAG laser with a pulse frequency of 10 Hz, a basic wavelength of 1,064 nm, a pulse duration of 7 ns, and an output power of 3.6 W was used for the ablation process. The metal plate was partially submerged inside a beaker containing 20 mL of the CS/PVA blend. To focus the laser beam on the metal target, the plate was moved in a direction perpendicular to the laser beam using a convex lens. The TEM images showed the fragmented spherical AuNPs scattered in CS/PVA solution with sizes of roughly 20 nm (Figure 2b). In summary, the liquid medium used in laser ablation, whether water or a CS/PVA blend, affects the temperature and chemical environment during the process, impacting the shape, size, and dispersion of synthesized AuNPs. Water assists in heat absorption and inhibits re-deposition, resulting in crystalline AuNPs with an average diameter of 10–25 nm, whereas the CS/PVA blend produces fragmented AuNPs scattered in solution, each around 20 nm in size. Further research into the unique impacts of various liquid media is required for a complete knowledge of laser ablation synthesis.

2.2 Chemical methods

The Turkevich method has long been considered the most well-known technique to synthesize colloidal AuNPs due to its simplicity, controllable size, and ease of synthesis.[7,50] This method uses sodium citrate as a reducing agent to reduce Au^{3+} ions in a heated environment.[7] The Turkevich method

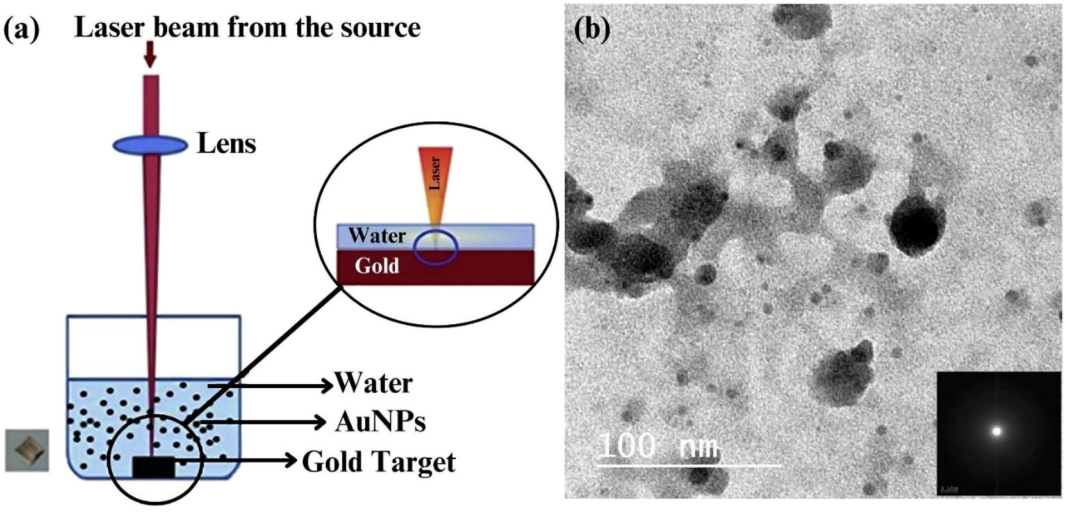

Figure 2: LAL synthesis AgNPs. (a) Schematic illustration of a typical water-submerged ablation system which is commonly utilized for synthesizing AuNPs[48] and (b) TEM images of AuNPs generated using a submerged laser ablation system using CS/PVA as the liquid medium. Adapted from ref. 49.

was used by Mintz et al.[51] to synthesize AuNPs with an average size of ~23 nm shown by AFM and TEM measurements (Figure 3). To synthesize AuNPs using the Turkevich method, a solution of sodium citrate is added to boiling aqueous solution of chloroauric acid ($HAuCl_4$) and mixture is vigorously stirred. A few minutes after stirring under boiling temperature, the mixture is cooled down in the dark. Like physical methods, AuNPs synthesized in a chemical manner had an absorbance peak of 525 nm. Using the concept presented by the Turkevich method, Sangamithirai et al.[52] achieved spherical AuNPs with a diameter of ~5 nm. $HAuCl_4$ aqueous solution was heated to boiling in a flask with continuous stirring, followed by the addition of sodium citrate. The mixture was then stirred for an additional 15 min under the same boiling setting until its color changed from pale yellow to red. The resulting citrate-stabilized AuNPs colloidal solution was slowly cooled to room temperature. The crystal patterns of AuNPs, identified using XRD, aligned with the JCPDS card no. 04-0784,[53] confirming the face-centered cubic polycrystalline structure. The crystallite size, calculated via the Scherrer equation, was approximately 5 nm, closely matching the size observed in high-resolution TEM images. Previous studies by Mintz et al. and Sangamithirai et al. utilized the Turkevich method with sodium citrate as a reducing agent. Sangamithirai et al., who preheated the $HAuCl_4$ solution, achieved smaller AuNPs (~5 nm) compared to Mintz et al.'s results (~23 nm). This approach likely optimized nucleation and growth dynamics, producing smaller and more uniform AuNPs.

Recent efforts have simplified the Turkevich method. For instance, it was found that incorporating sodium borohydride ($NaBH_4$) into the protocol, either with or without sodium citrate, can eliminate the heating step.[35] Utilizing this adaptation, Wang et al.[54] synthesized AuNPs with a diameter of 4 nm by adding sodium citrate to an $HAuCl_4$ solution at room temperature, followed by the addition of ice-chilled $NaBH_4$. The solution turned from colorless to red, indicating the formation of AuNPs, and, after stirring for 30 min, was left undisturbed for 2 h. The UV–vis spectrum showed a predominant SPR peak at 509 nm, with DLS indicating a hydrodynamic size of 6.3 nm and TEM calculating it at 5.0 nm. Following a similar method, Chaudhary et al.[55] synthesized AuNPs (7.53 nm) by mixing $HAuCl_4$ and sodium citrate solutions at room temperature, then adding $NaBH_4$ dropwise. The reddish color of the solution confirmed AuNP formation, and residual $NaBH_4$ was decomposed by stirring for 24 h. XRD and EDX analyses verified the face-centered cubic configuration of AuNPs, while Zeta potential measurements (~30 mV) indicated good stability.

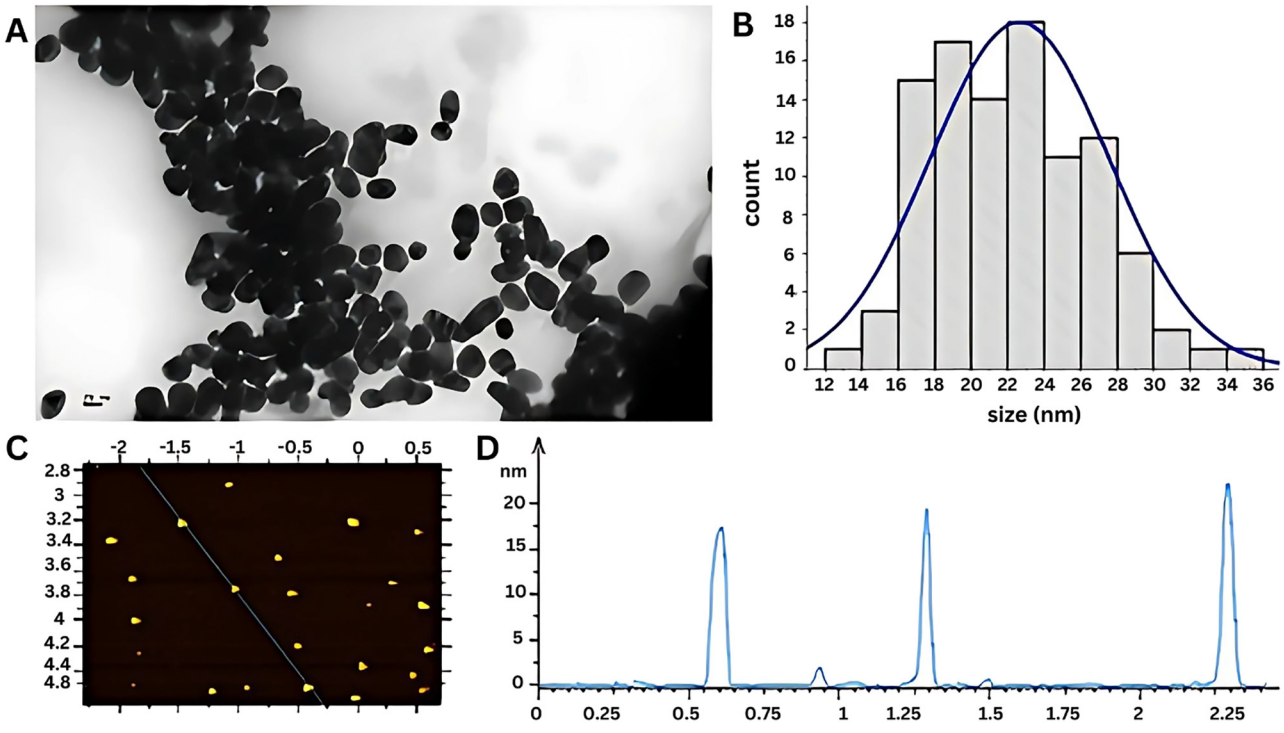

Figure 3: TEM image of AuNPs synthesized through Turkevich method (a); TEM-derived size distribution histogram showing an average diameter of ~ 23 nm (b); AFM image of the synthesized AuNPs through Turkevich method (c); and height profile generated from AFM image (d). Reprinted from ref. 51.

The Brust-Schiffrin method is another well-known technique to produce spherical AuNPs that are soluble in organic solvents.[35] The Brust-Schiffrin method is a two-phase process: (i) a phase transfer agent is used to transfer Au^{3+} ions from an aqueous-based to an organic-based phase. (ii) The organic-based Au^{3+} ions are then reduced through alkanethiol-mediated $NaBH_4$.[56] This method produces small-sized NPs (<10 nm) due to the strong affinity of thiol ligands on the Au surface, which prevents the self-assembly and aggregation of AuNPs.[35] Quintana et al.[57] combined aqueous solution of $HAuCl_4$ with tetraoctylammonium bromide (TOAB) – toluene as a new strategy to synthesize AuNPs. Dodecanethiol which served as a stabilizer, was then added to the mixture, and $AuCl^{4-}$ ions were reduced to AuNPs upon dropwise addition of $NaBH_4$. The organic solvent changed the color of the solution from orange to dark brown, implying the formation of AuNPs. The toluene (organic) phase was then removed from the water phase after further stirring for 30 min. The toluene phase was concentrated before being diluted with ethanol at the ratio of 1:200. The solution was kept at 22 °C for 2 h and was finally filtered through a nylon membrane and rinsed with ethanol. The TEM observation demonstrated tiny particles with an average size of 1.8 nm. In another study, Lee et al.[58] successfully synthesized 5-nm AuNPs by mixing aqueous $HAuCl_4$ with TOAB-toluene solution. After removing the aqueous phase, $NaBH_4$ was gradually added to the toluene phase. After stirring the mixture for 24 h, the toluene phase was collected and rinsed with sulfuric acid followed by deionized water. The aqueous solution was further stirred with an excess amount of dodecanethiol. The evaporation of toluene in the solution resulted in dried powder. To remove the unreacted reactants from AuNPs, the powder was uniformly distributed in chloroform and centrifuged at 25,000 rpm for 10 min. The powdered precipitate was then re-suspended in chloroform and stored at 4 °C.

The sonochemical method is a facile and rapid technique to obtain AuNPs. The operational mechanism of sonochemical method is to use a high-intensity ultrasound to molecules to initiate acoustic cavitation-induced chemical reactions.[59,60] When a liquid is exposed to ultrasound radiation, the periodic expansion and compression yield high- and low-pressure zones.[61] The presence of singular behavior in the liquid medium causes acoustic cavitation, which is the formation, expansion, and collapse of microbubbles.[59] Figure 4a illustrates the process of acoustic cavitation driven by ultrasonic radiation. After bubbles collapse, the pressure difference between the inner and outer sections of bubbles produces a shock wave.[62,63] In this context, ultrasonic waves cause better mechanical stirring than normal stirring.[64] The mechanical stirring, as along with the formation of high temperature and pressure caused by shock wave, collectively accelerate the radical formation and reduction of Au precursor.[64,65] There are many efforts dedicated to using ultrasound radiation to synthesize AuNPs. For example, Dheyab et al.[9] performed the sonochemical-assisted synthesis of AuNPs using the combined aqueous solution of $HAuCl_4$ and sodium citrate as precursors. The authors conducted the experiment by slowly adding 2 mL of 0.03 M $HAuCl_4$ solution into 20 mL of aqueous solution of 0.03 M sodium citrate. Sonication at a low frequency of 20 kHz and three different sonication powers (12, 20, and 36 W) were performed for 10 min to achieve complete mixing. XRD scans exhibited a single-face-centered cubic Au phase with high crystallinity. TEM size distribution measurements determined the diameters of spherical AuNPs to be 22.3, 18.6, and 13.6 nm for 12, 20, and 36 W power, respectively. With the increase of ultrasound power from 12 W to 36 W, the SPR peak shifted from 518 nm to 523 nm. The shift in the peak position of the UV–vis spectra from 518 nm to 523 nm indicates a redshift, which suggests an increase in particle size. In this context, it's a positive outcome as it correlates with enhanced catalytic activity, with the most effective catalysis observed when the gold nanoparticles were approximately 13.6 nm in size. The zeta potential was found

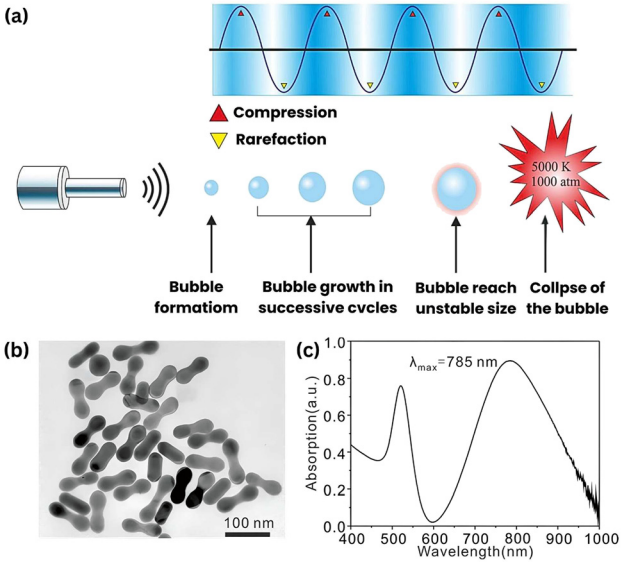

Figure 4: Chemical method synthesis AuNPs. (a) The process of the ultrasonic radiation that is used to generate acoustic signals for the synthesis of AuNPs. Reprinted from ref, 59. (b) TEM image of synthesized Au nanodumbbells; and (c) UV–vis spectral analysis of Au nanodumbbells, indicating the size-dependent optical properties of AuNPs. Adapted from ref. 66.

to be strongly dependent on sonication power. The zeta potentials of AuNPs were measured to be −35.7, −36.1, and −37.1 mV when sonication was conducted at an output power of 12, 20, and 36 W, respectively. These results suggested that increasing the sonication power from 12 W to 36 W led to much negative zeta potential and better water stability.

The seeding-growth method is another method to synthesize rod-shaped AuNPs. The reduction of an Au precursor governed by a reducing agent is performed to produce Au seed particles. Then, the single-crystal spherical Au seeds are grown into rod-like shape nanoparticles through a seed-mediated growth strategy.[35,50] Meng et al.[66] used this method to synthesize Au nanodumbbells from Au nanorods. $HAuCl_4$ as Au precursor reacted to cetyltrimethylammonium bromide (CTAB) solution at room temperature, followed by introducing ice–cold $NaBH_4$ solution, which turned the solution into a yellowish-brown color. The prepared seed solution was continuously stirred at 27 °C for 2 min to form a growth solution. The growth of Au nanorods can be controlled by the addition of CTAB to silver nitrate ($AgNO_3$) solution at room temperature. Next, $HAuCl_4$, nitric acid (HNO_3), and ascorbic acid were infused into the growth solution. The solution turned colorless from dark yellow. The seed solution was finally converted into the growth solution, creating Au nanorods with an aspect ratio of ~2.8. The Au nanorods were collected by centrifuging the colloidal solution at 8,000 rpm for 10 min for two cycles, discarding the supernatant liquid, and redispersing it in fresh CTAB solution. The growth solution of Au nanodumbbell was prepared by adding $HAuCl_4$ into CTAB and vigorously stirring at room temperature, followed by the addition of ascorbic acid. The color of the growth solution changed from yellow to colorless. The synthesis was concluded by adding nanorod seeds into the growth solution, producing Au nanodumbbells with a size of 86 nm in length, as seen from the TEM image (Figure 4b). The UV–vis spectral analysis revealed a broad SPR band at 785 nm and a lower absorption band around 530 nm due to the spherical AuNPs impurities and surface plasmons traveling across the transverse axis, respectively (Figure 4c). Nayef et al.[67] claimed that AuNPs of increasing sizes could be obtained with the increase in the volume of seed solution. Sodium citrate was included in the $HAuCl_4$ solution, followed by ice–cold $NaBH_4$. After 5 min of stirring, the seed solution was allowed to rest for 1 h at room temperature. The growth solution was made by combining $HAuCl_4$, CTAB, and ascorbic acid. Adding increasing amounts of seed solution (1 mL, 3 mL, and 10 mL) to the growth solution generated AuNPs of increasing sizes, which were 31.41 nm, 32.38 nm, and 47.86 nm, respectively (Table 1).

3 Green and sustainable synthesis of AuNPs

3.1 Green synthesis of AuNPs using bacteria

The bacterial biosynthesis of AuNPs could take place intracellularly or extracellularly where they are formed.[37] With the secretion of enzymes from bacteria, Au ions are enzymatically reduced to AuNPs. The enzyme-mediated reduction seems to be among the most convenient and environmentally friendly routes for synthesizing AuNPs.[27] The nitrate reductase is a typical enzyme that is crucial in the reduction of Au ions.[68,69] In the synthesis of AuNPs through the extracellular route, the surface-trapped Au ions are reduced with the presence of enzymes on the cell wall, whereas in the intracellular synthesis pathway, the Au ions are diffused into the cell that contains enzymes for their efficient reduction to AuNPs[31] (Figure 5).

The extracellular synthesis of AuNPs has attracted greater interest than intracellular synthesis because of the demand for fewer steps to release NPs.[13] Besides, AuNPs that are produced outside of cells through extracellular pathways do not have attached cellular components and, thus, can be used without purification for a variety of biomedical applications. The strengths of using bacteria for the synthesis of AuNPs lie in its simplicity of handling/operation, low cost, and efficiency.[71] However, despite the benefits, this technique has some drawbacks such as the inadequacy of control over the morphology and size of the AuNPs.[13] The underlying principles and molecular-level mechanisms to synthesize AuNPs using bacteria also are largely unknown. Several studies have attempted to understand these mechanisms at molecular levels to better control the size, shape, and crystallinity of AuNPs. For example, Patil et al.[72] managed to synthesize AuNPs with an average size of ~21 nm by using extracellular metabolites of *Paracoccus haeundaensis* BC74171^T, which is a marine bacterium. After incubation, the culture was centrifuged at 3,500 rpm for 30 min to separate the cells. $HAuCl_4$ and the collected supernatant were mixed and stirred magnetically in a heated water bath at 70 °C for 15 min, leading to the formation of AuNPs. The synthesized AuNPs were centrifuged, washed with distilled water, and finally freeze-dried to obtain powder form. The authors have shown the formation of AuNPs through XRD and EDX analyses. TEM observation revealed that the size of spherical AuNPs ranged between 15 and 35 nm. An SPR peak at 534 nm was found in the UV–vis spectrum, while the zeta potential of AuNPs was measured to be 4.26 mV. In another study, Markus et al.[73] used a probiotic

Table 1: Summary of selected studies focusing on AuNP synthesis via physical and chemical methods, detailing methods, chemicals used, particle shape and size, reaction times, characterization techniques, and target applications.

Method	Chemicals used	Shape/size	Reaction time	Characterization	Pros	Cons	Target application	Ref.
Physical method								
USP	$AuCl_4{\cdot}H_3O$, N_2, H_2, and sodium citrate	Spherical, polyhedron/ 20 nm	–	TEM, SEM, UV–vis, DLS	Versatile, high control over particle	Requires specialized equipment, high energy use	–	46
Ultrasonic spray pyrolysis	$HAuCl_4$, N_2, H_2, and PVP	Spherical/ 28 nm	–	STEM, TEM, DLS, UV–vis			Polyacrylate composites	42
Laser ablation	Organic solvent, chlorobenzene	Spherical/10–25 nm	–	XRD, FTIR, UV–vis, TEM	Pure products without stabilizers, high precision	Limited by laser costs, specific setups	–	48
Laser ablation	CS/PVA blend	Spherical/ 20 nm	10 min	XRD, FTIR, HRTEM, FESEM, UV–vis			Antibacterial device	49
Chemical method								
Turkevich	$HAuCl_4$, and sodium citrate	Spherical/ 23 nm	10 min	TEM, AFM, UV–vis	Simple, controllable size, stable	Limited to aqueous colloids, lower scalability	Tumor marker	51
Turkevich	$HAuCl_4$, and sodium citrate	Spherical/ 5 nm	15 min	XRD, HRTEM, XPS			Voltametric biosensor	52
Modified Turkevich	$HAuCl_4$, sodium citrate, and $NaBH_4$	–/4 nm	2.5 h	UV–vis, DLS, TEM			Detection of thiols and guanidine	54
Modified Turkevich	$HAuCl_4$, sodium citrate, and $NaBH_4$	Spherical/ 7.5 nm	24 h	UV–vis. XRD, FTIR, H NMR, DLS, TEM, EDX, zeta potential			siRNA delivery	55
Brust-Schiffrin	$HAuCl_4$, TOAB-toluene, $NaBH_4$, and dodecanethiol	Spherical/ 1.8 nm	–	SEM, TEM, XRD, DRS	Organic solvent compatibility, very small sizes	Longer processing time, organic solvent dependent	Electrode	57
Brust-Schiffrin	$HAuCl_4$, TOAB-toluene, $NaBH_4$, and dodecanethiol	Spherical/ 5 nm	26 h	DLS, TEM			Tumor treatment	58
Sonochemical	$HAuCl_4$, and sodium citrate	Spherical/ 13.6–22.3 nm	10 min	XRD, TEM, UV–vis, zeta potential	Rapid, environmentally friendly, scalable	Less control over morphology, cavitation requirements	Discoloration of methylene blue dye	9
Seeding-growth	$HAuCl_4$, CTAB, $NaBH_4$, $AgNO_3$, HNO_3, and ascorbic acid	Dumbbell/ 86 nm	–	FESEM, TEM, Raman spectrometer, UV–vis			Detection of prohibited colorants in drinks	66
Seeding-growth	$HAuCl_4$, sodium citrate, $NaBH_4$, CTAB, and ascorbic acid	Spherical/ 31.4–47.8 nm	1 h	UV–vis, FTIR, XRD, AFM,	Selective shape control, suitable for rod-like NPs	Requires multiple steps, longer setup	Organic vapor sensor	67

isolated from Korean kimchi, *Lactobacillus kimchicus* DCY51^T, to intracellularly synthesize spherical-shaped AuNPs with average particle sizes ranging from 5 nm to 30 nm (Figure 6). After sequential incubation and centrifugation, the collected cells were suspended in sterile water Followed by adding $AuCl_4H_3O$ into the suspension. The suspension was kept at 30 °C in the darkness. Visual examination for color change of the suspension was used to monitor the completeness of the AuNPs synthesis. The intracellularly synthesized AuNPs suspension was then centrifuged and underwent ultra-sonication several times before being rinsed with 80 % methanol to remove any unwanted or unreacted components. The powder form of AuNPs was finally collected by air-drying. The UV–vis

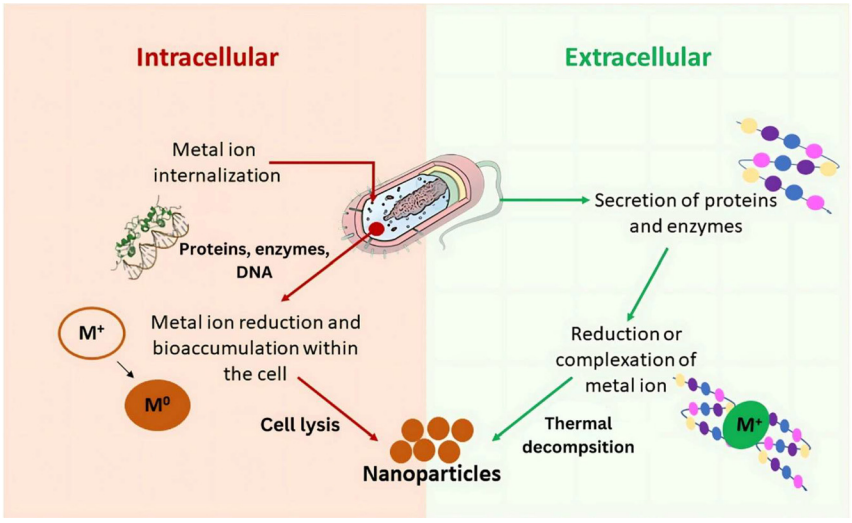

Figure 5: Schematic illustration of bacterial synthesis of AuNPs through intracellular and extracellular pathways. This figure demonstrates enzyme-driven reduction processes in bacterial synthesis of AuNPs, showing potential for environmentally friendly synthesis. Adapted from ref. 70.

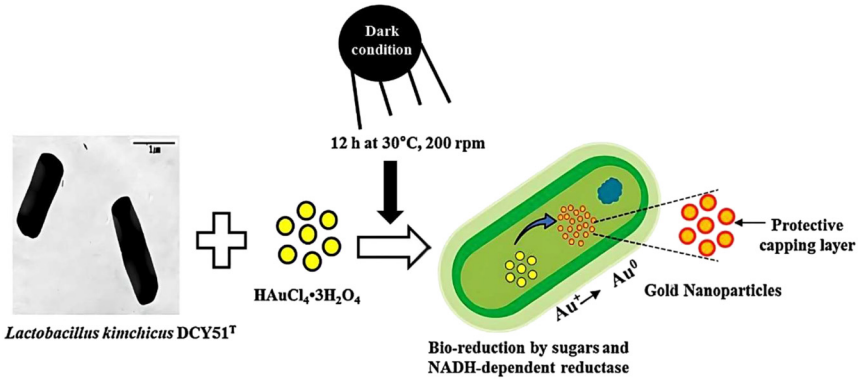

Figure 6: Formation of AuNPs through intracellular synthesis using *Lactobacillus kimchicus* DCY51^{T}, showing the role of bacterial processes in shaping AuNP size and morphology. Adapted from ref. 73.

showed an absorbance peak at ~540 nm. EDX analysis showed the presence of metallic Au as the major element in the sample, whereas XRD and SAED (Selected Area Electron Diffraction) confirmed the crystalline nature of the synthesized AuNPs.

3.2 Green synthesis of AuNPs using plant extracts

Plant species are an inexhaustible source of medicinal substances and have long been used for many medical practices.[37,74] As such, they have the potential to be used as a green-reducing agent for synthesizing AuNPs. Compared to bacteria-mediated synthesis, plant-mediated AuNP synthesis has a number of benefits, including the greater upscale potential by removing the time-consuming and costly stages of cell culturing.[36] It is interesting to note that a wide range of bio-compounds can take part in the biosynthesis of AuNPs, and these are abundant in plants. The chemical components of plants, such as flavonoids, phenols, quinones, and ketones, can reduce ions of precious metals, including Au, into NPs because these substances have many functional groups in their structure that can induce the stabilization and reduction of Au ions to AuNPs.[31,56] The hydroxyl groups present in polyphenols can be involved in the reduction of Au ions by their promotion to quinine forms, which follows Pearson's Hard and Soft Acids and Bases (HSAB) principles.[36] Based on these principles, soft acids prefer to coordinate with soft bases to produce covalent complexes, while hard bases choose to interact with hard acids to form ionic complexes. Indeed, the complex compound between a hard ligand and a soft metal (like Au^{+}) is very unlikely to be formed. Flavonoids are another compound present in plants that play a significant role in the green synthesis of AuNPs.[37] Flavonoids act as free radicals, transforming Au^{3+} ions to an intermediate complex, which is then oxidized to keto-form. The trivalent Au is finally reduced to AuNPs.

Using a green synthesis, palm (*Elaeis guineensis*) extract was used by Ahmad et al.[75] to synthesize AuNPs with an average diameter of ~ 28 nm. To remove the contaminations on the surfaces of the palm leaves, deionized water was used

to clean them. After being sun-dried for a week, the leaves were air-cleaned to remove any dust that might have appeared on them during drying. They were then oven-dried for 8 h at 70 °C and crushed to acquire fine leaves powder. After drying, 5 g of the powder were added to 100 mL of water, and the resulting mixture was heated to 70 °C while stirring for 10 min. The mixture was then filtered through Whatman filter paper. To synthesize AuNPs, an aqueous solution of $HAuCl_4$ and palm leaf extract was combined in a beaker. FTIR spectra of the extract and colloidal solution revealed the formation of functional groups that can contribute to the reduction of Au ions to AuNPs. The most prominent changes were the shifting of the O–H stretching band from 3,435 cm^{-1} to 3,450 cm^{-1}, confirming the presence of phenolic compounds. The shift of the stretching band associated with carboxylic and protein compounds at 1,634 cm^{-1} to 1,620 cm^{-1} was also demonstrated (Figure 7a). The majority of ofAuNPs had spherical shapes, with only a few AuNPs with triangular- and pentagonal shapes. In another study, Taib et al.[76] utilized *Hibiscus sabdariffa* leaf extract as the reducing agent for the synthesis of AuNPs. After washing the leaves with water, they were dried at 65 °C for 48 h. The dried leaves were then ground into powder. An aqueous solution was made by dissolving approximately 1 g of the powder into 100 mL of distilled water. After removing the solid content through filtration, a light, orange-colored extract with 3.1 pH was obtained. An aliquot of 10 mL leaves extract, and 10 mL of distilled water were combined and stirred under normal temperature while adding 5 mL $HAuCl_4{\cdot}3H_2O$ solution. The transformation of the solution from a pale orange to a purple color indicated the formation of AuNPs. The calculation of NPs particle size using TEM revealed an average size of 7 nm when stirring took 80 min. The pattern of XRD was similar to the established XRD patterns for AuNPs, and the crystallite size was calculated to be 6.96 nm. The authors proposed that the caffeic acid moiety of the phenol-chlorogenic acid, which is abundantly present in the leaves extract, caused the reduction of Au^{3+} ions to Au^0 (Figure 7b). The *ortho*-dihydroxyl groups of polyphenols that are converted to their oxidized form could stabilize the AuNPs.

3.3 Green synthesis of AuNPs using mushrooms

Mycomaterials are bio-compounds found in fungi like yeasts, molds, and mushrooms. The green synthesis of AuNPs from mycomaterials is referred to as myconanotechnology.[77] Mushrooms are considered another versatile natural source for the synthesis of AuNPs due to their widespread availability in nature.[77,78] A mushroom is a macro fungus with main parts visible to the naked eye.[79,80] Only a small portion of 20,000 types of mushrooms have been thoroughly studied, and they are mostly unknown. Edible mushrooms such as *Lentinus*, *Flammulina*, *Auricularia*, and *Pleurotus* sp. have been discovered to show therapeutic properties, including anticancer, antioxidant, and antitumor activities.

The presence of diverse substances such as tannins, polysaccharides, phenolic compounds, and terpenoids in biomaterials is beneficial in the production of AuNPs.[81] The primary advantage of using mushrooms as a natural precursor for NP synthesis is due to the rich content of extracellular enzymes, which can act as a stabilizing agent for AuNP synthesis. Most of the NPs synthesized by edible mushrooms occur through the extracellular pathway, which takes place outside the mushroom cells, and only a small percentage of synthesis occurs intracellularly in the hyphae of mushrooms.[82] Generally, mushroom-derived AuNPs have spherical shapes and sizes ranging from 0.4 nm to about 300 nm; the majority of particles have sizes of <75 nm.

Dheyab et al.[83] synthesized AuNPs using mushroom extract of *Agaricus bisporus,* which is commonly named Portobello mushroom. 20 g of freshly sliced Portobello mushrooms were used to make the watery extract. Mushrooms were first chopped and boiled in 150 mL of distilled water for 10 min. The crude solution was left to settle at 25 °C for a few minutes. Subsequently, the extract was purified using gauze and filter paper before being centrifuged for at 6,000 rpm 10 min 135 mL of $HAuCl_4$ was heated to 80 °C on a hot plate. Then, 15 mL of Portobello mushroom extract was mixed with the $HAuCl_4$ solution. After 30 min of stirring, the color of the mixture changed to pale magenta. When the mixture was further stirred for another 60 min, its color changed to a deep purple, and no further change was observed after. The FESEM exhibited the AuNPs with an average size of 53 nm and a variety of forms, including spherical, oval, triangular, drum-like, and hexagonal shapes. XRD patterns revealed the highest diffraction intensity at the (111) orientation, while UV–vis spectroscopy revealed the presence of an SPR peak at 568 nm. Another type of mushroom (*Laetiporus versisporus*), which is commonly called chicken of the woods, was used by Fathima et al. to synthesize AuNPs with a size of 10 nm. The fresh mushrooms were cleaned several times using water to remove the contaminants on the surface. The mushrooms are cut into small pieces and air-dried. The air-dried mushroom sample was then ground into powder. An aqueous solution of mushroom powder in distilled water was made, heated to boiling point, filtered, and cooled down to room temperature. The mushroom extract was mixed with $HAuCl_4$ solution. The mixture

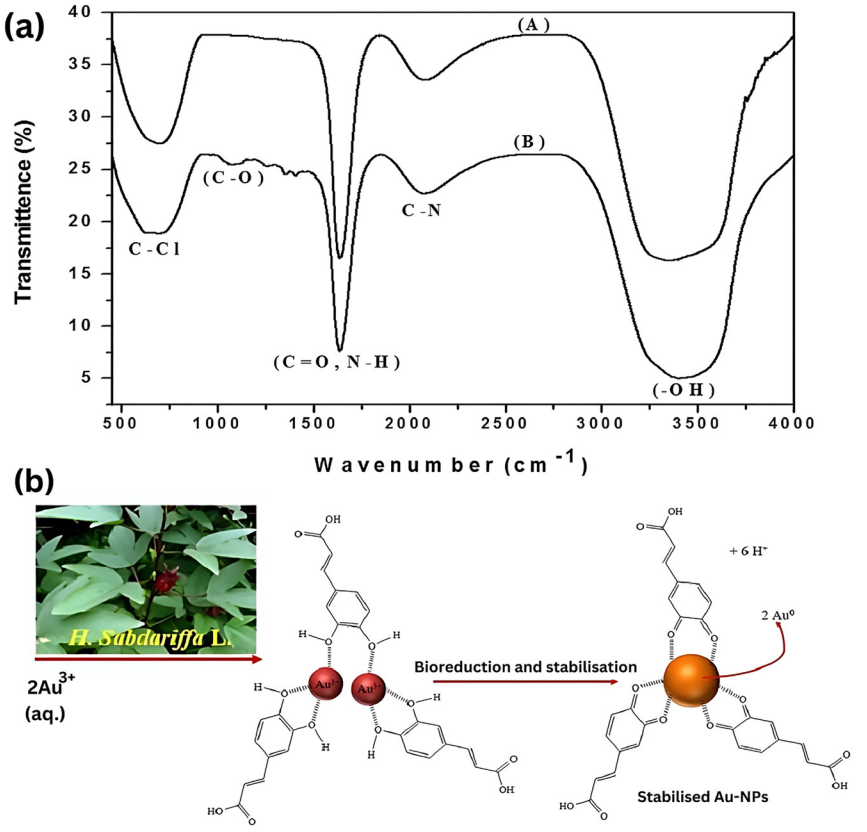

Figure 7: FTIR spectra of the AuNPs colloidal solution derived from *Elaeis guineensis* leaves extract,[75] the possible reduction and stabilization mechanism of Au^{3+} ions to Au^{0} induced by caffeic acid moiety present in *H. sabdariffa* L. extract. Adapted from ref. 76.

was left stirring in a dark place to achieve optimum reaction conditions. Stirring the mixture in this condition changed its original yellow color to a deep purple color. The purple AuNP product was centrifuged at 8,000 rpm for 10 min to separate the precipitate. The resulting precipitate was placed in hot air overnight to evaporate the water content, leading to the formation of AuNPs. The completeness of synthesis was done by UV–vis, which showed an absorbance peak of AuNPs at 566 nm, and TEM and SEM images, which clarified the spherical shape of AuNPs.

3.4 Green synthesis using algae

Algae are another novel source for the green synthesis of AuNPs. Algae are eukaryotic photoautotrophs that live in freshwater and oceanic habitats.[84] Algae are also classified as unicellular microalgae (green algae, diatoms, and golden algae) and multicellular macroalgae (green algae, brown algae, and red algae) (Figure 8). Algae have tremendous potential for the synthesis of AuNPs due to the existence of unique chemicals such as neutral glucan, fucoidan, and alginic acid that are absent in other natural organisms.[37] Algae are the fastest-growing organisms that are readily available in watery environments. Thus, a great advantage of using algae biomass as the reducing agent for the synthesis of AuNPs is their low-cost cultivation from water.[69] Algae offer abundant heavy metal binding sites, which facilitate metal absorption due to the existence of many hydroxyl groups in their subcomponents, such as proteins and polysaccharides (sulfated fucoidans).[37,69]

Senthilkumar et al.[86] used a red marine macroalgae (*Gelidiella acerosa*) to synthesize AuNPs. The algae were subsequently cleaned with clean water and deionized water to eliminate any contaminants and remaining salted materials on the surfaces, respectively. The cleaned algae were allowed to air-dry at room temperature for 2 weeks slowly. The dried algae were ground to powder using a household mixer. An aqueous solution was made by adding 5 g of algal powder to 100 mL of boiling distilled water. The resultant mixture underwent continuous stirring at 60 °C for 20 min. A Whatman filter paper was used to filter the green-colored watery extract. To synthesize AuNPs, 10 mL of the filtered extract was mixed with 90 mL of $HAuCl_4$ solution. Following that, the solution was maintained at 37 °C in a static condition. After 1 h of stirring with exposure to sunlight, the light-yellow color of $HAuCl_4$ solution changed to ruby red, indicating the generation of AuNPs. The sizes of particles ranged from 5.81 to 117.59 nm as confirmed from the high-resolution TEM. UV–vis spectroscopy analysis demonstrated the SPR

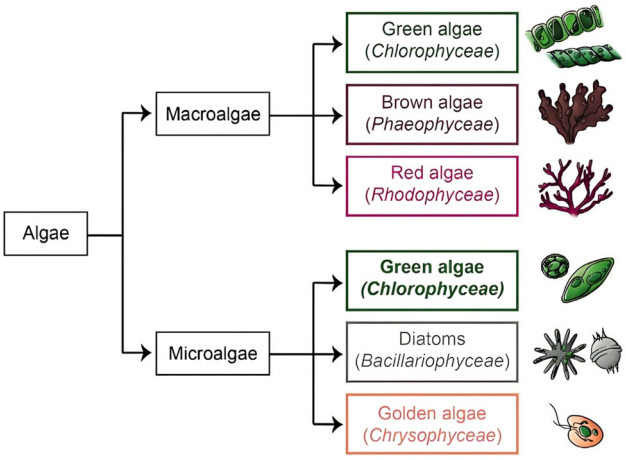

Figure 8: Classification of algae into macroalgae and microalgae based on photosynthetic pigments, illustrating diverse biological sources for green synthesis of AuNPs. Adapted from ref. 85.

peak at 526 nm (Figure 9). After a 3-month period, the UV–vis was retaken, yielding an almost identical peak at 526 nm, indicating the high stability of the solution over time. However, the intensity of this peak steadily grew, providing confirmation of the ongoing growth and development of the AuNPs. The authors proposed that the reasons behind the high stability of AuNPs could be due to the secondary metabolites present in the algae. The SEM investigation visualized the shapes of AuNPs in spherical, cubical, and hexagonal forms. In another research, AuNPs with an average diameter of 5 nm were synthesized by Suganya et al.[87] using blue-green algae (*Spirulina platensis*). 1 g of the powdered algae was combined with 10 mL of distilled water. After extraction and drying, the mixture was centrifuged at 5,000 rpm for 10 min to obtain the final extract. An aliquot of

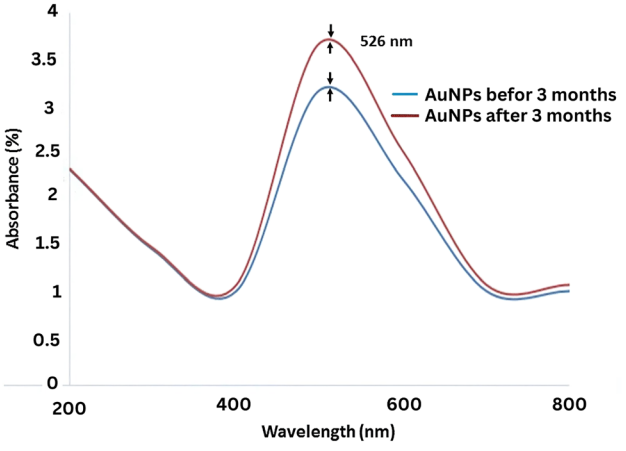

Figure 9: UV–vis analysis of AuNPs derived from *Gelidiella acerosa*, showing stability over a 3-month period, indicating the potential of algae-derived AuNPs for biomedical applications. Adapted from ref. 86.

10 mL extract was mixed with 10 mL of $HAuCl_4$ solution to initiate the AuNPs synthesis. Sodium hydroxide (NaOH) was then added to the extract/$HAuCl_4$ mixture while stirring. The addition of NaOH caused an immediate color shift from green to greenish-yellow. The stirring was continued at room temperature for 3 h before incubating for 48 h. The generation of AuNPs was visually confirmed by the appearance of a ruby-red color mixture. High-resolution TEM showed the monodispersed AuNPs with spherical shapes. FTIR and Raman analyses described the involvement of carboxylate, hydroxyl, and amine functional groups in the reduction and stabilization of AuNPs.

3.5 Green synthesis using yeasts

Yeasts are unicellular eukaryotic microfungi that can be found almost anywhere in any environment.[88] Indeed, they can be found in water, soil, fruits, skin surfaces, and even in the gastrointestinal tract of warm-blooded animals. These heterotrophic microorganisms can get their energy and nutrients from both living and dead residual organic matter. This high production of bio-compounds with carboxyl and amine groups, glycans, and sugars with reduction capability make yeasts a promising candidate for synthesizing AuNPs. In a similar mechanism to algae, yeasts can efficiently absorb and accumulate a wide range of heavy metal ions from their surroundings.[89] The reasonably simple nutrients needed for the rapid growth of yeasts and synthesis of enzymes, as well as the ease of culturing under laboratory conditions, made them preferable to bacteria for synthesizing AuNPs.[90]

Zhang et al.[91] used an isolated yeast from sea mud (*Magnusiomyces ingens*) to synthesize AuNPs, which had a size of ~80 nm. After incubation, the cells were centrifuged for 10 min at 10,000 g at 4 °C, washed two times with distilled water, and kept at −80 °C. To synthesize AuNPs, the yeast cells were subsequently resuspended in the water with a ratio of 2.2 and mixed with $HAuCl_4$ solution. The mixture was left stirring at 30 °C overnight. The mixture was then centrifuged at 3,000 g for 5 min to obtain the supernatant, which was filtered through a 0.45 µm syringe Millipore filter to eliminate cell fragments. UV–vis revealed a narrow absorbance peak that remained unchanged during reaction time, suggesting the existence of capping agents released by the yeast cells that prevent AuNPs agglomeration. The SEM and TEM studies showed diverse irregular morphologies, including sphere and plate-like (hexagon, triangle, pentagon) (Figure 10). Using a similar pathway, Rónavári et al.[92] used *Phaffia rhodozyma*, a kind of red yeast, to synthesize spherical AuNPs with extremely small size of 2.22 nm. The yeast cells were harvested after incubation for

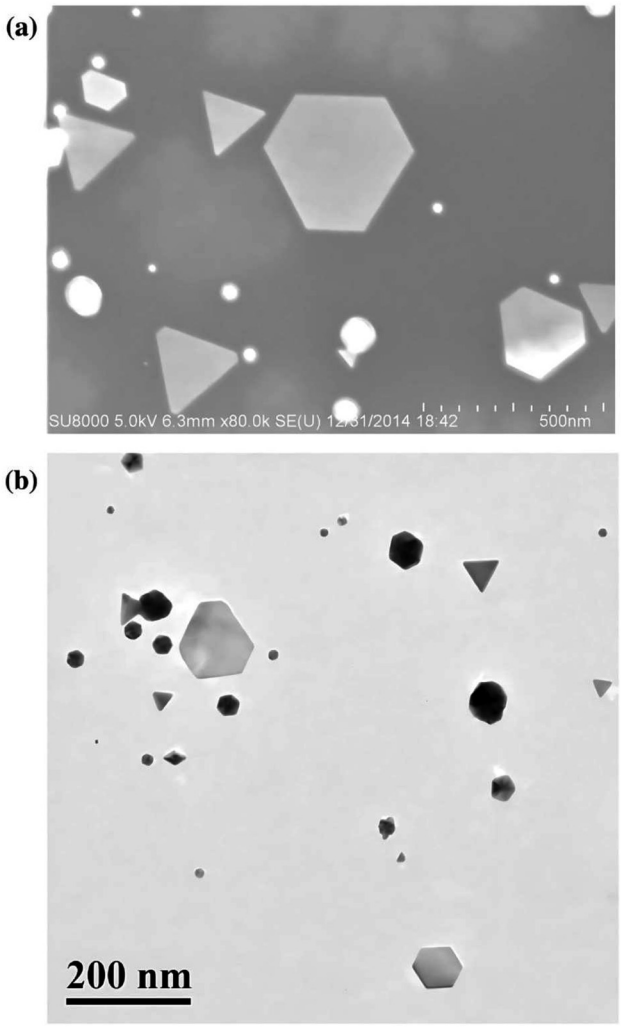

Figure 10: The SEM (a) and TEM (b) images of synthesized AuNPs by *Magnusiomyces ingens* LH-F1 yeasts. Adapted from ref. 91.

5 days. 10 g of fresh biomass was immersed in 200 mL of sterile water. The size of cells in water was broken down in a bead beater using glass beads. The small-sized cells were centrifuged for 15 min at 18,000 g at 4 °C to eliminate large cell fragments. The resulting product was then filtered through using a cellulose nitrate filter with pores of 0.45 µm. A similar protocol was used for synthesizing AuNPs. 10 mL of $HAuCl_4$ solution was added to 90 mL of extract to make a suspension. The suspension was continuously stirred at 22 °C overnight which led to the formation of NPs. The AuNPs were centrifuged at 18,000 g for 15 min at 4 °C and washed twice with distilled water. The synthesized spherical AuNPs were essentially monodispersed and well separated. The existence of SPR peak was confirmed at 541 nm, and the XRD analyses confirmed the crystalline patterns of AuNPs (Table 2).

4 Comparative analysis of synthesis methods for AuNPs

In comparing physical, chemical, and green synthesis methods, key distinctions emerge regarding size control, reaction conditions, scalability, and sustainability.

Physical methods such as ultrasonic spray pyrolysis (USP) and laser ablation require specialized equipment and are often limited by high energy input or specific reaction environments. However, they offer the advantage of fewer by-products and greater control over nanoparticle purity, especially with the laser ablation method, which does not require additional stabilizing agents. Conversely, chemical methods, especially the Turkevich and Brust-Schiffrin approaches, offer a more straightforward setup and can produce highly monodisperse AuNPs. The Turkevich method is particularly advantageous for producing stable, citrate-stabilized AuNPs in aqueous solutions, while Brust-Schiffrin enables AuNP synthesis in organic solvents for applications requiring hydrophobic particles. Each method thus holds unique advantages that make it suitable for different applications, such as tumor markers, electrode materials, or siRNA delivery systems.

Green synthesis methods, on the other hand, offer sustainable alternatives to conventional physical and chemical methods, emphasizing eco-friendly, low-toxicity approaches. Microorganism-mediated syntheses (using bacteria, fungi, algae, or yeast) provide advantages such as lower energy consumption and biocompatibility, making them suitable for biomedical applications. However, these methods can sometimes lack precise control over particle size and morphology compared to conventional methods. Plant extracts also serve as effective reducing and stabilizing agents, with additional functional benefits derived from bio-compounds, such as phenols and flavonoids, enhancing particle stability. Green synthesis methods thus hold unique promise for producing biocompatible AuNPs, though further optimization is required for achieving consistent particle size and morphology.

5 Medical applications of green-synthesized AuNPs

5.1 Antibacterial activities

Recent advancements in medicine have led to the development of new drugs for bacterial infections, yet the overuse of

Table 2: Summary of studies on green synthesis of AuNPs using various biological sources (bacteria, plants, mushrooms, algae, and yeasts), including synthesis conditions, particle characteristics, and applications.

Green reducing agent	Shape/size of AuNPs	Reaction time	Characterization tests	Target application	Ref.
Bacteria					
Paracoccus haeundaensis BC74171^T	Spherical/20.93 nm	15 min	UV–vis, TEM, zeta potential, XRD, FTIR	Antioxidant and antiproliferative activities	72
Lactobacillus kimchicus DCY51^T	Spherical/5–30 nm	12 h	UV–vis, FETEM, XRD, DLS, FTIR	Antioxidant activities	73
Plant extracts					
Elaeis guineensis	Spherical, triangular, and pentagonal/27.89 nm	10 min	FTIR, UV–vis, XRD, EDAX, XPS, FESEM, TEM, DLS	–	75
Hibiscus sabdariffa	Spherical/7 nm	80 min	UV–vis, XRD, TEM, FESEM, EDX, zeta potential, FTIR, ESI-TOF	Sensing nitrite ions	76
Mushrooms					
Agaricus bisporus	Spherical, oval, triangular, drum-like, and hexagonal/53 nm	2 h	UV–vis, AFM, FESEM, XRD, zeta potential, FTIR	Decolorization of MB dye	83
Laetiporus versisporus	Spherical/10 nm	–	UV–vis, FTIR, XRD, TEM, SEM	Antioxidant activities	78
Algae					
Gelidiella acerosa	Spherical, hexagonal, cubical/5.81–117.59 nm	1 h	HRTEM, UV–vis, SEM, XRD	Antidiabetic, antibacterial, and antioxidant activities	86
Spirulina platensis	Spherical/5 nm	51 h	UV–vis, fluorescence spectroscopy, FTIR, Raman spectroscopy, HRTEM, EDX	Antibacterial activities	87
Yeasts					
Magnusiomyces ingens LH-F1	Spherical, plates (hexagonal, triangular, pentagonal), irregular/80.1 nm	24 h	UV–vis, ICP-OES, SEM, TEM, DLS, FTIR	Catalyst for reduction of nitrophenols	91
Phaffia rhodozyma	Spherical/2.22 nm	24 h	TEM, DLS, XRD, UV–vis	Antifungal activities	92

multiple drugs has contributed to the rise of drug-resistant microorganisms, a serious public health concern.[19] This emphasizes the need to explore novel approaches, such as AuNPs, which offer potentially modifiable antibacterial properties. Green-synthesized AuNPs have shown promising antibacterial effects, potentially due to natural biocompounds present in plant or algae extracts that may enhance bactericidal action.[93] However, the antibacterial efficacy of AuNPs is influenced by various factors, including synthesis methods, AuNP concentrations, and bacterial strains.[94] Although positively charged AuNPs generally show high affinity for negatively charged bacterial cell surfaces, the degree of susceptibility varies between Gram-positive and Gram-negative bacteria due to differences in their cell wall structures.[37] Although all bacterial cells are negatively charged and have a high affinity to interact with positively charged AuNPs, Gram-negative bacteria are more vulnerable to AuNPs due to their thinner peptidoglycan layer than Gram-positive bacteria. Antibacterial action initially happens when AuNPs tightly attach to the bacteria's surface. This will lead to the destruction of flagella, visible damage to cell membranes, and reduced biofilm formation.[95]

For example, Suganya et al.[87] synthesized 5-nm spherical AuNPs using the blue-green algae (*S. platensis*) and showed their effective antibacterial activities against two Grain-positive bacteria, *Staphylococcus aureus (S. aureus)* and *Bacillus subtilis (B. subtilis)*. To assess the antibacterial activity, the zone of inhibition for each bacterium was measured (Figure 11), and vancomycin was used as the positive control. The antibacterial activity noticeably increased when the concentration of AuNPs increased. The

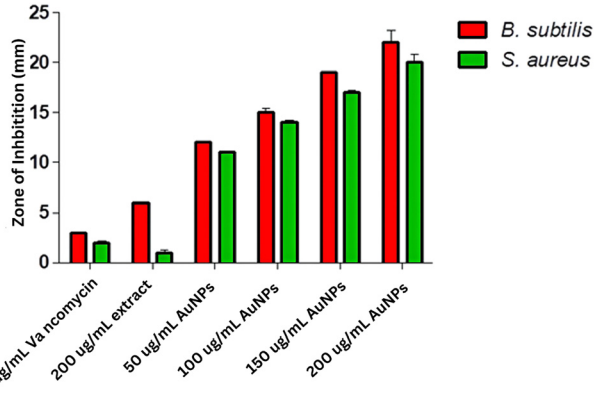

Figure 11: Zone of inhibition diameters for *B. subtilis* and *S. aureus* after exposure to varying AuNP concentrations, illustrating antibacterial efficacy. Adapted from ref. 87.

colony-forming unit (CFU) method was also used to evaluate the bactericidal capacity of AuNPs. The results showed the maximum reduction capability of 80.5 % and 97.4 % for *S. aureus* and *B. subtilis* colonies when treated with AuNPs of 150 µg/mL, respectively. However, as the authors expected, when colonies were exposed to higher concentrations of 200 µg/mL, a nearly complete reduction of 99 % was observed. Another representation of this concept was shown by Sunderam et al.[96] demonstrated that AuNPs synthesized with *Anacardium occidentale* leaves extract were effective against Gram-positive *B. subtilis* and Gram-negative *E. coli*, showing higher activity against *E. coli*. The differences in inhibition zones (8 and 10 mm for *B. subtilis*, and 18 and 24 mm for *E. coli*) reflect variations in bacterial susceptibility and suggest that further investigations are needed to understand the mechanisms driving these differences.

5.2 Anticancer activities

Cancer is a leading cause of death in humans. The number of different cancer cases has risen to an alarming level during the past years.[37] While nanotechnological breakthroughs have paved the way for countless methods for cancer diagnosis and therapy, most of these techniques showed potential side effects or drug reactions. As such, there is a tremendous potential to develop innovative drugs with minimal toxicity or side effects in a sustainable manner. Given the outstanding capacity of bio-compounds to readily adhere to the surfaces of AuNPs, the use of green synthesized AuNPs for treating tumors has been recommended.[97] This asset sets green synthesis apart from traditional ones in terms of its role in fighting against cancer. The remarkable ability of green synthesized AuNPs to permeate into tumor-bearing tissues is a great advantage that increases their likelihood of being utilized in cancer treatment.[98] It goes without saying that smaller AuNPs have stronger anticancer activities and greater renal clearance than large AuNPs. The AuNPs with relatively small sizes demonstrated better penetration into tumor tissue.[99] Using capping agents can unquestionably contribute to synthesizing AuNPs with robust antiproliferative activities that can disrupt cancer cell proteins or enzymatic activity.[37] The accumulation of AuNPs in cancer cells and the generation of reactive oxygen species (ROS) could induce cell apoptosis via intracellular oxidative stress.[100,101] For instance, AuNPs can increase the levels of ROS production in HeLa (human cervical cancer) cells and cause apoptotic cellular death through the mitochondrial-mediated pathway.[100]

Wu et al.[102] synthesized spherical AuNPs with a size of 200 nm from Siberian ginseng (*Eleutherococcus senticosus*).

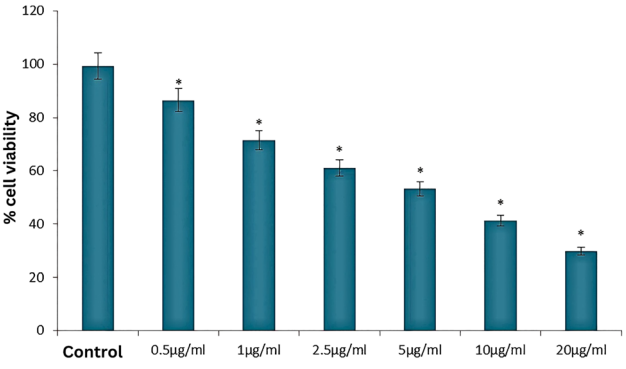

Figure 12: Anticancer activities of the green-synthesized AuNPs from *Siberian ginseng* against B16 cancer cells. Adapted from ref. 102.

The authors used different concentrations of AuNPs (0.5, 1, 2.5, 5, 10, and 20 µg/mL) to treat B16 murine melanoma cells both *in vitro* and *in vivo*. The treatment with AuNPs significantly decreased the number of viable cells. The reduction in the cell viability occurred in a dose-dependent fashion after exposure to a dosage of 0.5–20 µg/mL, with a 50 % reduction observed at the dose of 10 µg/ml AuNPs, as seen in Figure 12. Clarance et al.[103] used AuNPs synthesized from endophytic fungi (*Fusarium solani*) to evaluate their anticancer activities against HeLa cervical cancer cells, MCF-7 human breast cancer, and HEK human embryonic kidney cells. Cells were exposed to different concentrations of spindle-shaped AuNPs (0.5–4 µg/mL). The findings showed that AuNPs delivered anticancer properties against MCF-7 and HeLa cancer cell lines with IC_{50} values (half-maximal inhibitory concentration) of 0.8 µg/mL and 1.3 µg/mL, respectively. However, the findings showed negligible anticancer activities against HEK cancer cell lines. The irregular morphology of MCF-7 cell lines has likely resulted from the apoptotic fragmentation of cells. Hosny et al.[104] designed a study to compare the anticancer activities of spherical AuNPs synthesized using *Atriplex halimus* (2–10 nm) and *Chenopodium amperosidies* (up to 40 nm). AuNPs synthesized using *A. halimus* exhibited higher efficiency in reducing the growth of MCF-7 cell lines than those synthesized using *C. amperosidies*. The recorded cell viability IC_{50} values were 47.03 and 22 µg/mL for *A. halimus*-AuNPs and *C. amperosidies*-AuNPs, respectively.

5.3 Cancer imaging and diagnostic applications

The early diagnosis and detection of cancer is critical to reduce cancer mortality. Using AuNPs for cancer imaging is highly beneficial due to their distinctive capabilities such as light absorption and scattering characteristics.[17] Raman

imaging using non-emitting near-infrared wavelength is a common tool to visualize tumor-bearing tissues and track tumor progression. Using AuNPs in Raman imaging is very useful because the amplitude of the Raman signals on the AuNP surface is exceptionally high.[105] The high Raman signals of AuNPs stem from the presence of a broad SPR peak and the fast transfer of charges between the AuNP's surface and the target cancer cells. To enable better diagnosis or treatment follow-up and to obtain a more detailed image of tumors, computed tomography (CT) imaging is performed by intravenous injection of Iodinated contrast agents.[17] However, AuNPs have proven to be generally better than iodine-based contrast agents in terms of giving better contrast and imaging windows.[106] Other imaging procedures, such as positron emission tomography (PET) and magnetic resonance imaging (MRI), can also benefit from the development of AuNPs as targeted contrast agents. The site-specific accumulation of AuNPs in cancer cells can enable their early detection without side effects.

Morel et al.[107] used *Hypericum lanceolatum* (*H. lanceolatum*) as a traditional medicinal plant to synthesize flower-shaped AuNPs (40–80 nm). The potential application of plant-mediated AuNPs in visualizing cancer cells using CT-scan imaging was investigated. The author observed that *H. lanceolatum*-extract and citrate extract did not yield sufficient contrast to be visible on tumor images. In contrast, *H. lanceolatum*-derived AuNPs exhibited a strong contrast, as shown by the presence of a minor black deposit on the tube's base. The radiological contrast of the deposit was measured at around 621 HU, whereas that of the supernatant only showed 25 HU. Given these remarkable imaging features, the authors proposed that AuNPs could have promising potential to be used as photoacoustic contrast agents for multiple imaging modalities such as CT scans and MRI. Another study conducted by Uthaman et al.[108] used mannan (a bioactive polysaccharide derived from the cell walls of baker's yeast *Saccharomyces cerevisiae*) to synthesize spherical AuNPs with an average size of 9.18 nm. The authors first carried out CT phantom tests to examine the possible applications of AuNPs as a contrast agent for CT imaging, which showed a CT signal of 303 HU measured for AuNPs with a concentration of 20 mg/mL. Subcutaneous injection of AuNPs was inoculated into C57Bl/6 mice at the hindlimb footpads to understand the *in vivo* viability of AuNPs for lymph node CT imaging. It was found that injection of mannan-synthesized AuNPs into popliteal lymph nodes showed better contrast visibility than sodium citrate-synthesized AuNPs (Figure 13). The visible contrast of AuNPs on lymph nodes showed a time-dependent manner and significantly increased from 86 to 618 HU during 20 h of imaging. This observation clearly confirmed the effective diffusion of AuNPs from the injection site throughout the lymphatic system over time.

5.4 Targeted drug delivery and cancer therapy applications

AuNPs have contributed to modern medicine not only for cancer diagnostic applications but also for their ability to load high dosages of therapeutic agents and unload at the target cancer sites with enhanced therapeutic efficiency and much less adverse reactions.[18] The ability to customize AuNPs offers many opportunities for the creation of drug nanocarriers with varying diameters, shapes, and size distributions.[17,109] The large surface-area-to-volume ratio of AuNPs enables the efficient absorption of therapeutic agents onto their surface.[17] There are two methods to bind therapeutic agents onto the surface of AuNPs: (i) via linker molecules (also known as conjugation) and (ii) non-covalent bonds (also known as sorption). The versatility and controlled release of AuNP coatings with diverse therapeutic agents make them a promising nanoplatform for cancer treatment.[110]

Laksee et al. [111] synthesized spherical AuNPs with a diameter of 13.7 nm from pullulan. The potential of AuNPs,

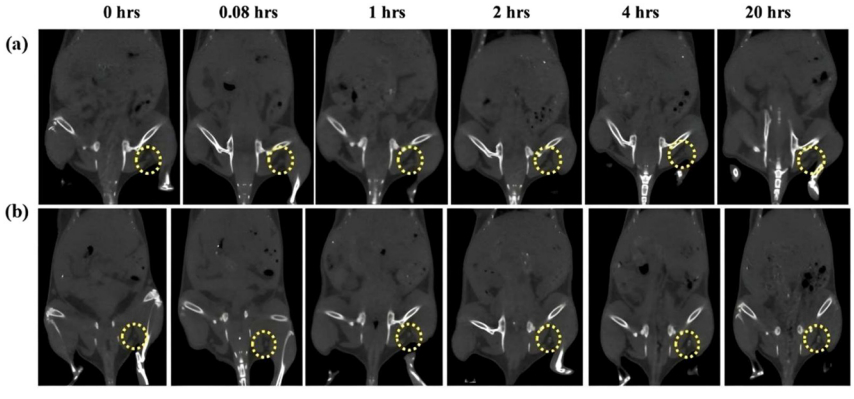

Figure 13: *In vivo* CT images of popliteal lymph nodes of mice that were injected with citrate-synthesized AuNPs (a) and mannan-synthesized AuNPs (b) over 20 h imaging period. Adapted from ref. 108.

which were conjugated with pullulan moieties (PM), was investigated for the targeted delivery of doxorubicin (DOX) as an anticancer drug without side effects. DOX-loaded AuNPs@PM was demonstrated to induce more apoptosis and higher anticancer activities against lung tumor cells than free DOX while exhibiting negligible cytotoxicity against normal lung cells. Malathi et al.[112] used chitosan to produce spherical AuNPs with sizes of 2–3 nm. They were then used as nanocarriers for the controlled release of an antibiotic, rifampicin (RIF), which is often used to treat tuberculosis. The drug loading efficiency of RIF-loaded AuNPs was calculated to be 71 %. The efficacy of RIF-loaded AuNPs exceeded that of free RIF in terms of antibacterial effectiveness because RIF-loaded AuNPs could better penetrate the cell walls of bacteria than free RIF. RIF-loaded AuNPs were reported to confer antibacterial action against both the Gram-negative (*Pseudomonas aeruginosa*) and Gram-positive (*B. subtilis*) bacteria.

5.5 Current clinical trials involving AuNPs

AuNPs have shown considerable promise in a variety of clinical applications due to their unique physicochemical properties and biocompatibility. In molecular imaging, AuNPs serve as effective contrast agents, particularly in photoacoustic imaging. With their high absorption cross-sections, AuNPs greater than 20 nm have proven effective in enhancing imaging contrast in *in vivo* models, although non-biodegradable properties can pose challenges, such as potential accumulation in organs like the spleen and liver.[113,114] However, recent studies have indicated that smaller, sub-10 nm AuNPs, which are comparable in size to biomolecules such as albumins and antibodies, may offer a solution to these issues by achieving highly uniform tissue distribution. In murine breast cancer models, these ultrasmall AuNPs demonstrated effective tissue penetration and distribution, positioning them as a promising option for sensitive and targeted *in vivo* imaging of cancer cells.[115]

In the realm of medical implants, AuNPs are being integrated to enhance osseointegration and reduce bacterial growth. For example, titanium implants coated with AuNPs (Ti-GNPs) have been shown to significantly promote osteogenic differentiation by upregulating mRNA expression specific to osteogenesis in human adipose-derived stem cells (ADSCs).[116] Additionally, studies using Ti-GNPs in animal models revealed improved osseous interface formation without signs of cytotoxicity, presenting AuNPs as an attractive option for enhancing implant performance and longevity. Further research on AuNP-mediated gene delivery is underway, focusing on its potential to improve bone formation in dental implants, even under conditions of osteoporosis.[117,118]

AuNPs have also been widely studied in diagnostics and biosensing. Their unique properties make them ideal for electrochemical immunosensors, as evidenced by clinical investigations for detecting disease markers such as Hepatitis B surface antigens and diphtheria toxins. In particular, AuNP-based platforms have demonstrated the ability to amplify the electrochemical signal of antibody-antigen interactions, enhancing the sensitivity and specificity of these diagnostic tools.[119] Paper-based devices incorporating AuNPs are also gaining attention for rapid, portable biomarker detection, with successful applications for identifying biomarkers of diseases like tuberculosis and infectious eye diseases using mechanisms like surface-enhanced Raman scattering (SERS) and colorimetric detection.[120,121]

In radiopharmaceuticals and nuclear medicine, AuNPs conjugated with radioisotopes such as Technetium-99m (Tc-99m) have been explored for both diagnostic and therapeutic uses, a field known as theranostics. One study demonstrated that Tc-99m-labeled AuNPs targeting atherosclerotic plaques enabled improved imaging diagnosis via SPECT/CT, with AuNPs showing enhanced blood circulation times and strong affinity to targeted sites.[122] Another investigation into Au nanoclusters containing radioactive isotopes illustrated their effectiveness in eradicating various cancer cell lines, such as melanoma and breast cancer, while also serving as PET imaging agents. These dual-function AuNPs radiopharmaceuticals are paving the way for simultaneous imaging and therapy applications in cancer treatment.[123,124]

Finally, AuNPs are proving invaluable in lab-on-a-chip technologies, where they are used in developing compact, efficient diagnostic devices. For instance, a recent clinical study integrated AuNPs into a lab-in-a-syringe system designed for immunosensing biomarkers, successfully detecting human IgG and PSA levels in spiked urine samples with high sensitivity.[125] Other lab-on-a-chip platforms utilizing AuNPs have enabled advancements in detecting environmental pollutants and biological markers, which may extend to critical healthcare applications such as viral and bacterial pathogen detection.[126]

These ongoing trials underscore the potential of AuNPs to enhance the sensitivity, specificity, and multifunctionality of diagnostic and therapeutic applications, marking significant steps toward clinical integration across diverse medical fields.

6 Limitations and challenges in green synthesized AuNPs for medical applications

Several challenges must be addressed before AuNPs synthesized via green methods can be effectively employed in biological contexts. Firstly, variations in natural extracts or plant materials utilized in these processes can lead to discrepancies in NP characteristics among different batches, necessitating standardized techniques for large-scale production and commercialization.[127] Secondly, while green synthesis techniques offer environmental benefits, they often lack precise control over NP size and morphology, emphasizing the importance of achieving uniformity in these aspects to ensure optimal performance in biomedical applications.[128] Initial steps in natural compound (NC) extraction involve sample preparation, method selection, and literature review, with researchers striving to minimize the presence of unwanted compounds that may co-extract with target molecules. Despite advancements in extraction methods, the quest for a universal technique remains ongoing, underscoring the complexity of isolating bioactive chemicals from natural sources.[129] Moreover, the stability of green-synthesized AuNPs under physiological conditions is paramount, necessitating strategies to prevent aggregation or instability, particularly in response to pH or temperature variations.[130] Surface modifications may further enhance stability, biocompatibility, and targeting capabilities, necessitating the development of reliable technologies for NP functionalization.[131,132] Although green synthesis is generally perceived as less harmful, long-term toxicity and biocompatibility studies are imperative to assess potential adverse effects on biological systems.[133,134] Lastly, scaling up production to meet biomedical demands presents logistical challenges, highlighting the need for scalable and cost-effective techniques that preserve NP characteristics. Addressing these multifaceted challenges is essential for the widespread application of green-synthesized AuNPs in biomedicine.[135]

7 Conclusions and future perspectives

With tremendous strides in nanotechnology, the green synthesis of AuNPs from renewable resources presents a sustainable pathway for developing innovative diagnostic and therapeutic tools for cancer treatment. This review highlights various green synthesis strategies, focusing on the physical, chemical, and structural properties of AuNPs. As thoroughly discussed in this review, combining green chemistry with conventional synthesis methods could provide ample opportunities for producing well-defined, homogeneous AuNPs with minimal environmental impact and low toxicity. Despite their tremendous potential, future research must address the challenges of controlling particle size, morphology, and scalability in green synthesis to improve consistency and efficacy. Investigating more refined green synthesis techniques, such as optimizing precursor concentrations or exploring novel biocompounds, could yield more uniform AuNPs with enhanced biomedical applications. Additionally, practical applications of green-synthesized AuNPs in cancer treatment need further exploration, particularly in targeted drug delivery and imaging. Studies on AuNPs as contrast agents for imaging techniques such as Raman, CT, and photoacoustic imaging show promise for early cancer detection with higher contrast than traditional agents. However, clinical translation requires robust studies on long-term biocompatibility, bio-distribution, and potential accumulation in non-target tissues. Future research should also explore the scalability of green synthesis methods to enable broader clinical and industrial applications. Collaborations between material scientists, chemists, and clinicians could help design AuNPs that are tailored to specific medical needs, including precision medicine and non-invasive diagnostics. Continued efforts to refine these nanoparticles for selective cancer targeting and controlled drug release mechanisms will enhance their therapeutic efficacy while minimizing adverse effects. As green-synthesized AuNPs evolve, their incorporation into cancer care protocols could significantly impact patient outcomes by providing sustainable, potent nanoscale solutions. A greater focus on safety assessments and sustainable production methods will be essential for translating these advances into clinical settings, ultimately revolutionizing cancer diagnosis and treatment.

Acknowledgments: The authors would like to extend their appreciation to Medical Physics and Biophysics Laboratory staff for their assistance and support.

Research ethics: Not applicable.

Informed consent: Not applicable.

Author contributions: Conceptualization, M.A.D. and A.A.A.; methodology, M.A.D., J.H.T.; software, M.A.D. J.H.T., N.O., and M.S.J; validation, M.A.D. M.G., and A.A.A.; formal analysis, M.A.D., J.H.T. N.O., M.S.J., M.A. and S.H.N.; investigation, M.A.D.; resources, M.A.D. M.A.; data curation, M.A.D., S.H.N.; writing – original draft preparation, M.A.D.; writing – review and editing, M.A.D. M.G. and A.A.A.; visualization,

M.A.D.; supervision, M.A.D and A.A.A.; project administration, M.A.D.; funding acquisition, M.A.D. All authors have accepted responsibility for the entire content of this manuscript and approved its submission.

Use of Large Language Models, AI and Machine Learning Tools: None declared.

Conflict of interest: The authors state no conflict of interest.

Research funding: The authors would like to extend their appreciation to Universiti Sains Malaysia (USM), Penang for the funding of this research (304/PFIZIK/6315745).

Data availability: Not applicable.

References

1. Hulla, J.; Sahu, S.; Hayes, A. Nanotechnology: History and Future. *Hum. Exp. Toxicol.* **2015**, *34* (12), 1318–1321.
2. Jameel, M. S.; Aziz, A. A.; Dheyab, M. A.; Mehrdel, B.; Khaniabadi, P. M.; Khaniabadi, B. M. Green Sonochemical Synthesis Platinum Nanoparticles as a Novel Contrast Agent for Computed Tomography. *Mater. Today Commun.* **2021**, *27*, 102480.
3. Jameel, M.; Abdul, A.; Ali, M.; Khaniabadi, P. M.; Kareem, A. A.; Alrosan, M.; Ali, A. T.; Rabeea, M. A.; Mehrdel, B. Mycosynthesis of Ultrasonically-Assisted Uniform Cubic Silver Nanoparticles by Isolated Phenols from Agaricus bisporus and its Antibacterial Activity. *Surface. Interfac.* **2022**, *29*, 101774.
4. Dheyab, M. A.; Aziz, A. A.; Jameel, M. S. Synthesis and Optimization of the Sonochemical Method for Functionalizing Gold Shell on Fe_3O_4 Core Nanoparticles Using Response Surface Methodology. *Surface. Interfac.* **2020**, *21*, 100647.
5. Dheyab, M. A.; Oladzadabbasabadi, N.; Aziz, A. A.; Khaniabadi, P. M.; Al-ouqaili, M. T.; Jameel, M. S.; Braim, F. S.; Mehrdel, B.; Ghasemlou, M. Recent Advances of Plant-Mediated Metal Nanoparticles: Synthesis, Properties, and Emerging Applications for Wastewater Treatment. *J. Environ. Chem. Eng.* **2024**, 112345; https://doi.org/10.1016/j.jece.2024.112345.
6. Dheyab, M. A.; Aziz, A. A.; Khaniabadi, P. M.; Jameel, M. S. Potential of a Sonochemical Approach to Generate MRI-PPT Theranostic Agents for Breast Cancer. *Photodiagnosis Photodyn. Ther.* **2021**, *33*, 102177.
7. Hammami, I.; Alabdallah, N. M.; Jomaa, A. A.; Kamoun, M. Gold Nanoparticles: Synthesis Properties and Applications. *J. King Saud Univ. Sci.* **2021**, *33* (7), 101560.
8. Ramsden, J. *Nanotechnology: An Introduction*; William Andrew, 2016.
9. Dheyab, M. A.; Abdul Aziz, A.; Jameel, M. S.; Moradi Khaniabadi, P.; Mehrdel, B. Sonochemical-Assisted Synthesis of Highly Stable Gold Nanoparticles Catalyst for Decoloration of Methylene Blue Dye. *Inorg. Chem. Commun.* **2021**, *127*, 108551.
10. Dheyab, M. A.; Abdul Aziz, A.; Moradi Khaniabadi, P.; Jameel, M. S.; Ahmed, N. M.; Taha Ali, A. Distinct Advantages of Using Sonochemical over Laser Ablation Methods for a Rapid-High Quality Gold Nanoparticles Production. *Mater. Res. Express* **2021**, *8* (1), 015009.
11. Mehrdel, B.; Othman, N.; Aziz, A. A.; Khaniabadi, P. M.; Jameel, M. S.; Dheyab, M. A.; Amiri, I. S. Identifying Metal Nanoparticle Size Effect on Sensing Common Human Plasma Protein by Counting the Sensitivity of Optical Absorption Spectra Damping. *Plasmonics* **2020**, *15*, 123–133.
12. Dheyab, M. A.; Aziz, A. A.; Oladzadabbasabadi, N.; Alsaedi, A.; Braim, F. S.; Jameel, M. S.; Ramizy, A.; Alrosan, M.; Almajwal, A. M. Comparative Analysis of Stable Gold Nanoparticles Synthesized Using Sonochemical and Reduction Methods for Antibacterial Activity. *Molecules* **2023**, *28* (9), 3931.
13. Kalimuthu, K.; Cha, B. S.; Kim, S.; Park, K. S. Eco-Friendly Synthesis and Biomedical Applications of Gold Nanoparticles: A Review. *Microchem. J.* **2020**, *152*, 104296.
14. Meena, J.; Gupta, A.; Ahuja, R.; Panda, A. K.; Bhaskar, S. Inorganic Particles for Delivering Natural Products. In *Sustainable Agriculture Reviews 44: Pharmaceutical Technology for Natural Products Delivery Vol. 2 Impact of Nanotechnology*; Springer Nature: Switzerland, 2020; pp 205–241.
15. Bolaños, K.; Kogan, M. J.; Araya, E. Capping Gold Nanoparticles with Albumin to Improve Their Biomedical Properties. *Int. J. Nanomed.* **2019**, 6387–6406; https://doi.org/10.2147/ijn.s210992.
16. Bai, X.; Wang, Y.; Song, Z.; Feng, Y.; Chen, Y.; Zhang, D.; Feng, L. The Basic Properties of Gold Nanoparticles and Their Applications in Tumor Diagnosis and Treatment. *Int. J. Mol. Sci.* **2020**, *21* (7), 2480.
17. Vodyashkin, A. A.; Rizk, M. G. H.; Kezimana, P.; Kirichuk, A. A.; Stanishevskiy, Y. M. Application of Gold Nanoparticle-Based Materials in Cancer Therapy and Diagnostics. *ChemEngineering* **2021**, *5* (4), 69.
18. Khanna, P.; Kaur, A.; Goyal, D. Algae-Based Metallic Nanoparticles: Synthesis, Characterization and Applications. *J. Microbiol. Methods* **2019**, *163*, 105656.
19. Tepale, N.; Fernández-Escamilla, V. V. A.; Carreon-Alvarez, C.; González-Coronel, V. J.; Luna-Flores, A.; Carreon-Alvarez, A.; Aguilar, J. Nanoengineering of Gold Nanoparticles: Green Synthesis, Characterization, and Applications. *Crystals* **2019**, *9* (12), 612.
20. Anik, M. I.; Mahmud, N.; Al Masud, A.; Hasan, M. Gold Nanoparticles (GNPs) in Biomedical and Clinical Applications: A Review. *Nano Sel.* **2022**, *3* (4), 792–828.
21. Yao, L.; Bojic, D.; Liu, M. Applications and Safety of Gold Nanoparticles as Therapeutic Devices in Clinical Trials. *J. Pharm. Anal.* **2023**, *13* (9), 960–967.
22. Tudda, A.; Donzelli, E.; Nicolini, G.; Semperboni, S.; Bossi, M.; Cavaletti, G.; Castriconi, R.; Mangili, P.; Vecchio, A. d.; Sarno, A.; Mettivier, G.; Russo, P. Breast Radiotherapy with Kilovoltage Photons and Gold Nanoparticles as Radiosensitizer: An In Vitro Study. *Med. Phys.* **2022**, *49* (1), 568–578.
23. Oumano, M.; Russell, L.; Salehjahromi, M.; Shanshan, L.; Sinha, N.; Ngwa, W.; Yu, H. CT Imaging of Gold Nanoparticles in a Human-Sized Phantom. *J. Appl. Clin. Med. Phys.* **2021**, *22* (1), 337–342.
24. Zare, A.; Shamshiripour, P.; Lotfi, S.; Shahin, M.; Rad, V. F.; Moradi, A. R.; Hajiahmadi, F.; Ahmadvand, D. Clinical Theranostics Applications of Photo-Acoustic Imaging as a Future Prospect for Cancer. *J. Contr. Release* **2022**, *351*, 805–833.
25. Mehrnia, S. S.; Hashemi, B.; Mowla, S. J.; Nikkhah, M.; Arbabi, A. Radiosensitization of Breast Cancer Cells Using AS1411 Aptamer-Conjugated Gold Nanoparticles. *Radiat. Oncol.* **2021**, *16*, 1–12.
26. Khaniabadi, P. M.; Ahmed, N. M.; Dheyab, M. A.; Aziz, A. A.; Almessiere, M. Structure, Morphology and Absorption Characteristics of Gold Nanoparticles Produced via PLAL Method: Role of Low Energy X-Ray Dosage. *Surface. Interfac.* **2021**, *24*, 101139.
27. Ghosh, S.; Ahmad, R.; Zeyaullah, M.; Khare, S. K. Microbial Nano-Factories: Synthesis and Biomedical Applications. *Front. Chem.* **2021**, *9*, 626834.
28. Bloch, K.; Pardesi, K.; Satriano, C.; Ghosh, S. Bacteriogenic Platinum Nanoparticles for Application in Nanomedicine. *Front. Chem.* **2021**, *9*, 624344.
29. Lin, L.; Starostin, S. A.; Li, S.; Hessel, V. Synthesis of Metallic Nanoparticles by Microplasma. *Phys. Sci. Rev.* **2018**, *3* (10), 20170121.

30. Slepička, P.; Slepičková Kasálková, N.; Siegel, J.; Kolská, Z.; Švorčík, V. Methods of Gold and Silver Nanoparticles Preparation. *Materials* **2019**, *13* (1), 1.
31. Jiang, Z.; Li, L.; Huang, H.; He, W.; Ming, W. Progress in Laser Ablation and Biological Synthesis Processes: "Top-Down" and "Bottom-Up" Approaches for the Green Synthesis of Au/Ag Nanoparticles. *Int. J. Mol. Sci.* **2022**, *23* (23), 14658.
32. Aswathi, V.; Meera, S.; Maria, C. G. A.; Nidhin, M. Green Synthesis of Nanoparticles from Biodegradable Waste Extracts and Their Applications: A Critical Review. *Nanotechnol. Environ. Eng.* **2022**, 1–21; https://doi.org/10.1007/s41204-022-00276-8.
33. Dheyab, M. A.; Abdul Aziz, A.; Hussein Nowfal, S.; Al-Mafarjy, S. S.; Abdullah, W.; Suardi, N.; Jameel, M. S.; Braim, F. S.; Alrosan, M.; Khaniabadi, P. M. Turning Food Waste-Derived Ultrasmall Gold Nanoparticles as a Photothermal Agent for Breast Cancer Cell Eradication. *Inorg. Chem. Commun.* **2024**, *169*, 113030.
34. Rabeea, M. A.; Naeem, G. A.; Owaid, M. N.; Abdul Aziz, A.; Jameel, M. S.; Dheyab, M. A.; Muslim, R. F.; Jameel, L. F. Phytosynthesis of Prosopis Farcta Fruit-Gold Nanoparticles Using Infrared and Thermal Devices and Their Catalytic Efficacy. *Inorg. Chem. Commun.* **2021**, *133*, 108931.
35. De Souza, C. D.; Nogueira, B. R.; Rostelato, M. E. C. Review of the Methodologies Used in the Synthesis Gold Nanoparticles by Chemical Reduction. *J. Alloys Compd.* **2019**, *798*, 714–740.
36. Sengani, M.; Grumezescu, A. M.; Rajeswari, V. D. Recent Trends and Methodologies in Gold Nanoparticle Synthesis–A Prospective Review on Drug Delivery Aspect. *OpenNano* **2017**, *2*, 37–46.
37. Mikhailova, E. O. Gold Nanoparticles: Biosynthesis and Potential of Biomedical Application. *J. Funct. Biomater.* **2021**, *12* (4), 70.
38. Dheyab, M. A.; Aziz, A. A.; Khaniabadi, P. M.; Jameel, M. S.; Oladzadabbasabadi, N.; Rahman, A. A.; Braim, F. S.; Mehrdel, B. Gold Nanoparticles-Based Photothermal Therapy for Breast Cancer. *Photodiagnosis Photodyn. Ther.* **2023**, *42*, 103312.
39. Dheyab, M. A.; Aziz, A. A.; Moradi Khaniabadi, P.; Jameel, M. S.; Oladzadabbasabadi, N.; Mohammed, S. A.; Abdullah, R. S.; Mehrdel, B. Monodisperse Gold Nanoparticles: A Review on Synthesis and Their Application in Modern Medicine. *Int. J. Mol. Sci.* **2022**, *23* (13), 7400.
40. Alizadeh, S.; Nazari, Z. A Review on Gold Nanoparticles Aggregation and its Applications. *J. Chem. Rev.* **2020**, *2* (4), 228–242.
41. Mitri, N.; Rahme, K.; Fracasso, G.; Ghanem, E. Upgrading Gold to Green Nanoparticles: Applications in Prostate Cancer. *Adv. Nat. Sci. Nanosci. Nanotechnol.* **2023**, *14* (2), 023001.
42. Golub, D.; Ivanič, A.; Majerič, P.; Tiyyagura, H. R.; Anžel, I.; Rudolf, R. Synthesis of Colloidal Au Nanoparticles Through Ultrasonic Spray Pyrolysis and Their Use in the Preparation of Polyacrylate-AuNPs' Composites. *Materials* **2019**, *12* (22), 3775.
43. Majerič, P.; Jenko, D.; Friedrich, B.; Rudolf, R. Formation Mechanisms for Gold Nanoparticles in a Redesigned Ultrasonic Spray Pyrolysis. *Adv. Powder Technol.* **2017**, *28* (3), 876–883.
44. Shariq, M.; Friedrich, B.; Budic, B.; Hodnik, N.; Ruiz-Zepeda, F.; Majerič, P.; Rudolf, R. Successful Synthesis of Gold Nanoparticles Through Ultrasonic Spray Pyrolysis from a Gold (III) Nitrate Precursor and Their Interaction with a High Electron Beam. *ChemistryOpen* **2018**, *7* (7), 533–542.
45. Majerič, P.; Rudolf, R. Advances in Ultrasonic Spray Pyrolysis Processing of Noble Metal Nanoparticles. *Materials* **2020**, *13* (16), 3485.
46. Bekić, M.; Tomić, S.; Rudolf, R.; Milanović, M.; Vučević, D.; Anžel, I.; Čolić, M. The Effect of Stabilisation Agents on the Immunomodulatory Properties of Gold Nanoparticles Obtained by Ultrasonic Spray Pyrolysis. *Materials* **2019**, *12* (24), 4121.
47. Abid, N.; Khan, A. M.; Shujait, S.; Chaudhary, K.; Ikram, M.; Imran, M.; Haider, J.; Khan, M.; Khan, Q.; Maqbool, M. Synthesis of Nanomaterials Using Various Top-Down and Bottom-Up Approaches, Influencing Factors, Advantages, and Disadvantages: A Review. *Adv. Colloid Interface Sci.* **2022**, *300*, 102597.
48. Al-Shamari, A.; Abdelghany, A.; Alnattar, H.; Oraby, A. Structural and Optical Properties of PEO/CMC Polymer Blend Modified with Gold Nanoparticles Synthesized by Laser Ablation in Water. *J. Mater. Res. Technol.* **2021**, *12*, 1597–1605.
49. Menazea, A.; Ahmed, M. Wound Healing Activity of Chitosan/Polyvinyl Alcohol Embedded by Gold Nanoparticles Prepared by Nanosecond Laser Ablation. *J. Mol. Struct.* **2020**, *1217*, 128401.
50. Elahi, N.; Kamali, M.; Baghersad, M. H. Recent Biomedical Applications of Gold Nanoparticles: A Review. *Talanta* **2018**, *184*, 537–556.
51. Mintz, K.; Waidely, E.; Zhou, Y.; Peng, Z.; Al-Youbi, A. O.; Bashammakh, A. S.; El-Shahawi, M. S.; Leblanc, R. M. Carbon Dots and Gold Nanoparticles Based Immunoassay for Detection of Alpha-L-Fucosidase. *Anal. Chim. Acta* **2018**, *1041*, 114–121.
52. Sangamithirai, D.; Munusamy, S.; Narayanan, V.; Stephen, A. A Voltammetric Biosensor Based on Poly (O-methoxyaniline)-Gold Nanocomposite Modified Electrode for the Simultaneous Determination of Dopamine and Folic Acid. *Mater. Sci. Eng. C* **2018**, *91*, 512–523.
53. Mishra, A. N.; Bhadauria, S.; Gaur, M. S.; Pasricha, R.; Kushwah, B. S. Synthesis of Gold Nanoparticles by Leaves of Zero-Calorie Sweetener Herb (Stevia rebaudiana) and Their Nanoscopic Characterization by Spectroscopy and Microscopy. *Int. J. Green Nanotechnol. Phys. Chem.* **2010**, *1* (2), P118–P124.
54. Wang, Y.; Wang, M.; Zhao, Y.; Fan, A. Enhancement Effect of p-Iodophenol on Gold Nanoparticle-Catalyzed Chemiluminescence and its Applications in Detection of Thiols and Guanidine. *Talanta* **2018**, *182*, 523–528.
55. Chaudhary, A.; Garg, S. siRNA Delivery Using Polyelectrolyte-Gold Nanoassemblies in Neuronal Cells for BACE1 Gene Silencing. *Mater. Sci. Eng. C* **2017**, *80*, 18–28.
56. Shah, M.; Badwaik, V.; Kherde, Y.; Waghwani, H.K.; Modi, T.; Aguilar, Z.P.; Rodgers, H.; Hamilton, W.; Marutharaj, T.; Webb, C.; Lawrenz, M.B.; Dakshinamurthy, R. Gold Nanoparticles: Various Methods of Synthesis and Antibacterial Applications. *Front. Biosci.-Landmark* **2014**, *19* (8), 1320–1344.
57. Quintana, C.; Atienzar, P.; Budroni, G.; Mora, L.; Hernández, L.; García, H.; Corma, A. Development and Characterization of Fluorine Tin Oxide Electrodes Modified with High Area Porous Thin Films Containing Gold Nanoparticles. *Thin Solid Films* **2010**, *519* (1), 487–493.
58. Lee, J. M.; Youn, Y. S.; Lee, E. S. Development of Light-Driven Gas-Forming Liposomes for Efficient Tumor Treatment. *Int. J. Pharm.* **2017**, *525* (1), 218–225.
59. Dheyab, M. A.; Aziz, A. A.; Jameel, M. S.; Khaniabadi, P. M.; Mehrdel, B. Mechanisms of Effective Gold Shell on Fe_3O_4 Core Nanoparticles Formation Using Sonochemistry Method. *Ultrason. Sonochem.* **2020**, *64*, 104865.
60. Ali Dheyab, M.; Abdul Aziz, A.; Jameel, M. S.; Moradi Khaniabadi, P.; Oglat, A. A. Rapid Sonochemically-Assisted Synthesis of Highly Stable Gold Nanoparticles as Computed Tomography Contrast Agents. *Appl. Sci.* **2020**, *10* (20), 7020.
61. Acisli, O.; Khataee, A.; Darvishi Cheshmeh Soltani, R.; Karaca, S. Ultrasound-Assisted Fenton Process Using Siderite Nanoparticles Prepared via Planetary Ball Milling for Removal of Reactive Yellow 81 in Aqueous Phase. *Ultrason. Sonochem.* **2017**, *35*, 210–218.

62. Nomura, H.; Koda, S. What Is Sonochemistry? In *Sonochemistry and the Acoustic Bubble*; Elsevier: Amsterdam, 2015; pp 1–9.
63. Johansen, K.; Song, J. H.; Prentice, P. Performance Characterisation of a Passive Cavitation Detector Optimised for Subharmonic Periodic Shock Waves from Acoustic Cavitation in MHz and Sub-MHz Ultrasound. *Ultrason. Sonochem.* **2018**, *43*, 146–155.
64. Jameel, M. S.; Aziz, A. A.; Dheyab, M. A.; Mehrdel, B.; Khaniabadi, P. M. Rapid Sonochemically-Assisted Green Synthesis of Highly Stable and Biocompatible Platinum Nanoparticles. *Surface. Interfac.* **2020**, *20*, 100635.
65. Susanna, D.; Balakrishnan, R. M.; Ettiyappan, J. P. Ultrasonication-Assisted Green Synthesis and Characterization of Gold Nanoparticles from Nothapodytes Foetida: An Assessment of Their Antioxidant, Antibacterial, Anticancer and Wound Healing Potential. *J. Drug Deliv. Sci. Technol.* **2023**, 104740; https://doi.org/10.1016/j.jddst.2023.104740.
66. Meng, J.; Qin, S.; Zhang, L.; Yang, L. Designing of a Novel Gold Nanodumbbells SERS Substrate for Detection of Prohibited Colorants in Drinks. *Appl. Surf. Sci.* **2016**, *366*, 181–186.
67. Nayef, U. M.; Khudhair, I. M. Synthesis of Gold Nanoparticles Chemically Doped with Porous Silicon for Organic Vapor Sensor by Using Photoluminescence. *Optik* **2018**, *154*, 398–404.
68. Lee, K. X.; Shameli, K.; Yew, Y. P.; Teow, S. Y.; Jahangirian, H.; Rafiee-Moghaddam, R.; Webster, T. Recent Developments in the Facile Bio-Synthesis of Gold Nanoparticles (AuNPs) and Their Biomedical Applications. *Int. J. Nanomed.* **2020**, 275–300; https://doi.org/10.2147/ijn.s233789.
69. Menon, S.; Rajeshkumar, S.; Kumar, V. A Review on Biogenic Synthesis of Gold Nanoparticles, Characterization, and its Applications. *Resour.-Effic. Technol.* **2017**, *3* (4), 516–527.
70. Bandeira, M.; Giovanela, M.; Roesch-Ely, M.; Devine, D. M.; da Silva Crespo, J. Green Synthesis of Zinc Oxide Nanoparticles: A Review of the Synthesis Methodology and Mechanism of Formation. *Sustainable Chem. Pharm.* **2020**, *15*, 100223.
71. Kalishwaralal, K.; Deepak, V.; Ram Kumar Pandian, S.; Gurunathan, S. Biological Synthesis of Gold Nanocubes from Bacillus Licheniformis. *Bioresour. Technol.* **2009**, *100* (21), 5356–5358.
72. Patil, M. P.; Kang, M. j.; Niyonizigiye, I.; Singh, A.; Kim, J. O.; Seo, Y. B.; Kim, G. D. Extracellular Synthesis of Gold Nanoparticles Using the Marine Bacterium Paracoccus Haeundaensis BC74171T and Evaluation of Their Antioxidant Activity and Antiproliferative Effect on Normal and Cancer Cell Lines. *Colloids Surf. B Biointerfaces* **2019**, *183*, 110455.
73. Markus, J.; Mathiyalagan, R.; Kim, Y. J.; Abbai, R.; Singh, P.; Ahn, S.; Perez, Z. E. J.; Hurh, J.; Yang, D. C. Intracellular Synthesis of Gold Nanoparticles with Antioxidant Activity by Probiotic Lactobacillus Kimchicus DCY51T Isolated from Korean Kimchi. *Enzym. Microb. Technol.* **2016**, *95*, 85–93.
74. Al-Mafarjy, S. S.; Suardi, N.; Ahmed, N. M.; Kernain, D.; Hisham Alkatib, H.; Dheyab, M. A. Green Synthesis of Gold Nanoparticles from Coleus Scutellarioides (L.) Benth Leaves and Assessment of Anticancer and Antioxidant Properties. *Inorg. Chem. Commun.* **2024**, *161*, 112052.
75. Ahmad, T.; Bustam, M. A.; Irfan, M.; Moniruzzaman, M.; Anwaar Asghar, H. M.; Bhattacharjee, S. Green Synthesis of Stabilized Spherical Shaped Gold Nanoparticles Using Novel Aqueous Elaeis Guineensis (Oil Palm) Leaves Extract. *J. Mol. Struct.* **2018**, *1159*, 167–173.
76. Taib, S. H. M.; Shameli, K.; Moozarm Nia, P.; Etesami, M.; Miyake, M.; Rasit Ali, R.; Abouzari-Lotf, E.; Izadiyan, Z. Electrooxidation of Nitrite Based on Green Synthesis of Gold Nanoparticles Using Hibiscus sabdariffa Leaves. *J. Taiwan Inst. Chem. Eng.* **2019**, *95*, 616–626.
77. Rabeea, M. A.; Owaid, M. N.; Aziz, A. A.; Jameel, M. S.; Dheyab, M. A. Mycosynthesis of Gold Nanoparticles Using the Extract of Flammulina Velutipes, Physalacriaceae, and Their Efficacy for Decolorization of Methylene Blue. *J. Environ. Chem. Eng.* **2020**, *8* (3), 103841.
78. Farzana Fathima, M.; Usha Raja Nanthini, A.; Al-Khattaf, F. S.; Hatamleh, A. A.; Kabir, S. B. Mycosynthesis of Noble Metal Nanoparticle Using Laetiporus Versisporus Mushroom and Analysis of Antioxidant Activity. *J. Nanomater.* **2022**, *2022*; https://doi.org/10.1155/2022/8086803.
79. Chopra, H.; Goyal, R.; Agarwal, N.; Mishra, D.; Gautam, R.K. Edible Mushroom Assisted Synthesis and Applications of Metal Nanoparticles: A Comprehensive Review. *J. Integrated Sci. Technol.* **2023**, *11* (1), 427.
80. Dheyab, M. A.; Aziz, A. A.; Al-Mafarjy, S. S.; Suardi, N.; Razak, N. N. A. N. A.; Ramizy, A.; Jameel, M. S. Exploring the Anticancer Potential of Biogenic Inorganic Gold Nanoparticles Synthesized via Mushroom-Assisted Green Route. *Inorg. Chem. Commun.* **2023**, *157*, 111363.
81. Eskandari-Nojedehi, M.; Jafarizadeh-Malmiri, H.; Rahbar-Shahrouzi, J. Hydrothermal Green Synthesis of Gold Nanoparticles Using Mushroom (Agaricus bisporus) Extract: Physico-Chemical Characteristics and Antifungal Activity Studies. *Green Process. Synth.* **2018**, *7* (1), 38–47.
82. Owaid, M. N.; Ibraheem, I. J. Mycosynthesis of Nanoparticles Using Edible and Medicinal Mushrooms. *Eur. J. Nanomed.* **2017**, *9* (1), 5–23.
83. Dheyab, M. A.; Owaid, M. N.; Rabeea, M. A.; Aziz, A. A.; Jameel, M. S. Mycosynthesis of Gold Nanoparticles by the Portabello Mushroom Extract, Agaricaceae, and Their Efficacy for Decolorization of Azo Dye. *Environ. Nanotechnol. Monit. Manag.* **2020**, *14*, 100312.
84. Kouzuma, A.; Watanabe, K. Exploring the Potential of Algae/Bacteria Interactions. *Curr. Opin. Biotechnol.* **2015**, *33*, 125–129.
85. Nzayisenga, J. C. *Autotrophic and heterotrophic culture of Nordic microalgae in wastewater for lipid production*; Umeå University: Umeå, 2020.
86. Senthilkumar, P.; Surendran, L.; Sudhagar, B.; Ranjith Santhosh Kumar, D. S. Facile Green Synthesis of Gold Nanoparticles from Marine Algae Gelidiella acerosa and Evaluation of its Biological Potential. *SN Appl. Sci.* **2019**, *1*, 1–12.
87. Suganya, K. U.; Govindaraju, K.; Ganesh Kumar, V.; Stalin Dhas, T.; Karthick, V.; Singaravelu, G.; Elanchezhiyan, M. Blue Green Alga Mediated Synthesis of Gold Nanoparticles and its Antibacterial Efficacy Against Gram Positive Organisms. *Mater. Sci. Eng. C* **2015**, *47*, 351–356.
88. Shurson, G. Yeast and Yeast Derivatives in Feed Additives and Ingredients: Sources, Characteristics, Animal Responses, and Quantification Methods. *Anim. Feed Sci. Technol.* **2018**, *235*, 60–76.
89. Gahlawat, G.; Choudhury, A. R. A Review on the Biosynthesis of Metal and Metal Salt Nanoparticles by Microbes. *RSC Adv.* **2019**, *9* (23), 12944–12967.
90. Saravanan, A.; Kumar, P. S.; Karishma, S.; Vo, D. V. N.; Jeevanantham, S.; Yaashikaa, P.; George, C. S. A Review on Biosynthesis of Metal Nanoparticles and its Environmental Applications. *Chemosphere* **2021**, *264*, 128580.
91. Zhang, X.; Qu, Y.; Shen, W.; Wang, J.; Li, H.; Zhang, Z.; Li, S.; Zhou, J. Biogenic Synthesis of Gold Nanoparticles by Yeast Magnusiomyces ingens LH-F1 for Catalytic Reduction of Nitrophenols. *Colloids Surf. A Physicochem. Eng. Asp.* **2016**, *497*, 280–285.
92. Rónavári, A.; Igaz, N.; Gopisetty, M. K.; Szerencsés, B.; Kovács, D.; Papp, C.; Vágvölgyi, C.; Boros, I.; Kónya, Z.; Kiricsi, M.; Pfeiffer, I. Biosynthesized Silver and Gold Nanoparticles Are Potent Antimycotics against Opportunistic Pathogenic Yeasts and Dermatophytes. *Int. J. Nanomed.* **2018**, *13*, 695.

93. Nagalingam, M.; Kalpana, V. N.; Panneerselvam, A. Biosynthesis, Characterization, and Evaluation of Bioactivities of Leaf Extract-Mediated Biocompatible Gold Nanoparticles from Alternanthera bettzickiana. *Biotechnol. Rep.* **2018**, *19*, e00268.
94. Wani, I. A.; Ahmad, T. Size and Shape Dependant Antifungal Activity of Gold Nanoparticles: A Case Study of Candida. *Colloids Surf., B* **2013**, *101*, 162–170.
95. Geethalakshmi, R.; Sarada, D. Gold and Silver Nanoparticles from Trianthema Decandra: Synthesis, Characterization, and Antimicrobial Properties. *Int. J. Nanomed.* **2012**, 5375–5384; https://doi.org/10.2147/ijn.s36516.
96. Sunderam, V.; Thiyagarajan, D.; Lawrence, A. V.; Mohammed, S. S. S.; Selvaraj, A. In-vitro Antimicrobial and Anticancer Properties of Green Synthesized Gold Nanoparticles Using Anacardium occidentale Leaves Extract. *Saudi J. Biol. Sci.* **2019**, *26* (3), 455–459.
97. Akintelu, S. A.; Yao, B.; Folorunso, A. S. Bioremediation and Pharmacological Applications of Gold Nanoparticles Synthesized from Plant Materials. *Heliyon* **2021**, *7* (3), e06591.
98. Fan, M.; Han, Y.; Gao, S.; Yan, H.; Cao, L.; Li, Z.; Liang, X. J.; Zhang, J. Ultrasmall Gold Nanoparticles in Cancer Diagnosis and Therapy. *Theranostics* **2020**, *10* (11), 4944.
99. Huang, K.; Ma, H.; Liu, J.; Huo, S.; Kumar, A.; Wei, T.; Zhang, X.; Jin, S.; Gan, Y.; Wang, P. C.; Zhang, X.; Liang, X. J. Size-Dependent Localization and Penetration of Ultrasmall Gold Nanoparticles in Cancer Cells, Multicellular Spheroids, and Tumors In Vivo. *ACS Nano* **2012**, *6* (5), 4483–4493.
100. Ke, Y.; Al Aboody, M. S.; Alturaiki, W.; Alsagaby, S. A.; Alfaiz, F. A.; Veeraraghavan, V. P.; Mickymaray, S. Photosynthesized Gold Nanoparticles from Catharanthus Roseus Induces Caspase-Mediated Apoptosis in Cervical Cancer Cells (HeLa). *Artif. Cells, Nanomed. Biotechnol.* **2019**, *47* (1), 1938–1946.
101. Yun, Z.; Chinnathambi, A.; Alharbi, S. A.; Jin, Z. Biosynthesis of Gold Nanoparticles Using Vetex Negundo and Evaluation of Pro-apoptotic Effect on Human Gastric Cancer Cell Lines. *J. Photochem. Photobiol. B Biol.* **2020**, *203*, 111749.
102. Wu, F.; Zhu, J.; Li, G.; Wang, J.; Veeraraghavan, V. P.; Krishna Mohan, S.; Zhang, Q. Biologically Synthesized Green Gold Nanoparticles from Siberian Ginseng Induce Growth-Inhibitory Effect on Melanoma Cells (B16). *Artif. Cells, Nanomed. Biotechnol.* **2019**, *47* (1), 3297–3305.
103. Clarance, P.; Luvankar, B.; Sales, J.; Khusro, A.; Agastian, P.; Tack, J. C.; Al Khulaifi, M. M.; Al-Shwaiman, H. A.; Elgorban, A. M.; Syed, A.; Kim, H. J. Green Synthesis and Characterization of Gold Nanoparticles Using Endophytic Fungi Fusarium Solani and its In-Vitro Anticancer and Biomedical Applications. *Saudi J. Biol. Sci.* **2020**, *27* (2), 706–712.
104. Hosny, M.; Fawzy, M.; Abdelfatah, A. M.; Fawzy, E. E.; Eltaweil, A. S. Comparative Study on the Potentialities of Two Halophytic Species in the Green Synthesis of Gold Nanoparticles and Their Anticancer, Antioxidant and Catalytic Efficiencies. *Adv. Powder Technol.* **2021**, *32* (9), 3220–3233.
105. Ielo, I.; Rando, G.; Giacobello, F.; Sfameni, S.; Castellano, A.; Galletta, M.; Drommi, D.; Rosace, G.; Plutino, M. R. Synthesis, Chemical–Physical Characterization, and Biomedical Applications of Functional Gold Nanoparticles: A Review. *Molecules* **2021**, *26* (19), 5823.
106. Kim, J.; Lee, N.; Hyeon, T. Recent Development of Nanoparticles for Molecular Imaging. *Phil. Trans. Math. Phys. Eng. Sci.* **2017**, *375* (2107), 20170022.
107. Morel, A.-L.; Giraud, S.; Bialecki, A.; Moustaoui, H.; de La Chapelle, M. L.; Spadavecchia, J. Green Extraction of Endemic Plants to Synthesize Gold Nanoparticles for Theranostic Applications. *Front. Lab. Med.* **2017**, *1* (3), 158–171.
108. Uthaman, S.; Kim, H. S.; Revuri, V.; Min, J. J.; Lee, Y. k.; Huh, K. M.; Park, I. K. Green Synthesis of Bioactive Polysaccharide-Capped Gold Nanoparticles for Lymph Node CT Imaging. *Carbohydr. Polym.* **2018**, *181*, 27–33.
109. Duncan, B.; Kim, C.; Rotello, V. M. Gold Nanoparticle Platforms as Drug and Biomacromolecule Delivery Systems. *J. Contr. Release* **2010**, *148* (1), 122–127.
110. Rana, S.; Bajaj, A.; Mout, R.; Rotello, V. M. Monolayer Coated Gold Nanoparticles for Delivery Applications. *Adv. Drug Deliv. Rev.* **2012**, *64* (2), 200–216.
111. Laksee, S.; Puthong, S.; Kongkavitoon, P.; Palaga, T.; Muangsin, N. Facile and Green Synthesis of Pullulan Derivative-Stabilized Au Nanoparticles as Drug Carriers for Enhancing Anticancer Activity. *Carbohydr. Polym.* **2018**, *198*, 495–508.
112. Malathi, S.; D. Balakumaran, M.; T. Kalaichelvan, P.; Balasubramanian, S. Green Synthesis of Gold Nanoparticles for Controlled Delivery. *Adv. Mater. Lett.* **2013**, *4* (12), 933–940.
113. Weber, J.; Beard, P. C.; Bohndiek, S. E. Contrast Agents for Molecular Photoacoustic Imaging. *Nat. Methods* **2016**, *13* (8), 639–650.
114. Han, S.; Bouchard, R.; Sokolov, K. V. Molecular Photoacoustic Imaging with Ultra-Small Gold Nanoparticles. *Biomed. Opt Express* **2019**, *10* (7), 3472–3483.
115. Chen, F.; Ma, K.; Madajewski, B.; Zhuang, L.; Zhang, L.; Rickert, K.; Marelli, M.; Yoo, B.; Turker, M. Z.; Overholtzer, M.; Quinn, T. P.; Gonen, M.; Zanzonico, P.; Tuesca, A.; Bowen, M. A.; Norton, L.; Subramony, J. A.; Wiesner, U.; Bradbury, M. S. Ultrasmall Targeted Nanoparticles with Engineered Antibody Fragments for Imaging Detection of HER2-Overexpressing Breast Cancer. *Nat. Commun.* **2018**, *9* (1), 4141.
116. Li, H.; Pan, S.; Xia, P.; Chang, Y.; Fu, C.; Kong, W.; Yu, Z.; Wang, K.; Yang, X.; Qi, Z. Advances in the Application of Gold Nanoparticles in Bone Tissue Engineering. *J. Biol. Eng.* **2020**, *14*, 1–15.
117. Ko, W.-K.; Kim, S. J.; Heo, D. N.; Han, I. B.; Kim, S.; Kwon, I. K.; Sohn, S. Double Layers of Gold Nanoparticles Immobilized Titanium Implants Improve the Osseointegration in Rabbit Models. *Nanomed. Nanotechnol. Biol. Med.* **2020**, *24*, 102129.
118. Singh, S.; Gupta, A.; Qayoom, I.; Teotia, A. K.; Gupta, S.; Padmanabhan, P.; Dev, A.; Kumar, A. Biofabrication of Gold Nanoparticles with Bone Remodeling Potential: An In Vitro and In Vivo Assessment. *J. Nanoparticle Res.* **2020**, *22* (6), 152.
119. Xue, Q.; Bian, C.; Tong, J.; Sun, J.; Zhang, H.; Xia, S. FET Immunosensor for Hemoglobin A1c Using a Gold Nanofilm Grown by a Seed-Mediated Technique and Covered with Mixed Self-Assembled Monolayers. *Microchim. Acta* **2012**, *176*, 65–72.
120. Tsai, T.-T.; Huang, C. Y.; Chen, C. A.; Shen, S. W.; Wang, M. C.; Cheng, C. M.; Chen, C. F. Diagnosis of Tuberculosis Using Colorimetric Gold Nanoparticles on a Paper-Based Analytical Device. *ACS Sens.* **2017**, *2* (9), 1345–1354.
121. Zhang, H.; Yi, Y.; Zhou, C.; Ying, G.; Zhou, X.; Fu, C.; Zhu, Y.; Shen, Y. SERS Detection of microRNA Biomarkers for Cancer Diagnosis Using Gold-Coated Paramagnetic Nanoparticles to Capture SERS-Active Gold Nanoparticles. *RSC Adv.* **2017**, *7* (83), 52782–52793.
122. Li, X.; Wang, C.; Tan, H.; Cheng, L.; Liu, G.; Yang, Y.; Zhao, Y.; Zhang, Y.; Li, Y.; Zhang, C.; Xiu, Y.; Cheng, D.; Shi, H. Gold Nanoparticles-Based SPECT/CT Imaging Probe Targeting for Vulnerable Atherosclerosis Plaques. *Biomaterials* **2016**, *108*, 71–80.
123. Xuan, S.; de Barros, A. O. D. S.; Nunes, R. C.; Ricci-Junior, E.; da Silva, A. X.; Sahid, M.; Alencar, L. M. R.; dos Santos, C. C.; Morandi, V.; Alexis, F.; Iram, S. H.; Santos-Oliveira, R. Radioactive Gold Nanocluster (198-AuNCs) Showed Inhibitory Effects on Cancer Cells Lines. *Artif. Cell Nanomed. Biotechnol.* **2020**, *48* (1), 1214–1221.

124. Lee, S. B.; Ji, H. D.; Lee, I. K.; Kim, K. S.; Lee, J.; Jeon, Y. H. Visualization of Platelet Recruitment to Tumor Lesions Using Highly Sensitive and Stable Radioiodine Studded Gold Nanoprobes. *J. Mater. Chem. B* **2021**, *9* (12), 2931–2936.
125. Chamorro-Garcia, A.; de la Escosura-Muñiz, A.; Espinoza-Castañeda, M.; Rodriguez-Hernandez, C. J.; de Torres, C.; Merkoçi, A. Detection of Parathyroid Hormone-like Hormone in Cancer Cell Cultures by Gold Nanoparticle-Based Lateral Flow Immunoassays. *Nanomed. Nanotechnol. Biol. Med.* **2016**, *12* (1), 53–61.
126. Markandan, K.; Tiong, Y. W.; Sankaran, R.; Subramanian, S.; Markandan, U. D.; Chaudhary, V.; Numan, A.; Khalid, M.; Walvekar, R. Emergence of Infectious Diseases and Role of Advanced Nanomaterials in Point-Of-Care Diagnostics: A Review. *Biotechnol. Genet. Eng. Rev.* **2022**, 1–89; https://doi.org/10.1080/02648725.2022.2127070.
127. Saleh, T. A.; Fadillah, G. Green Synthesis Protocols, Toxicity, and Recent Progress in Nanomaterial-Based for Environmental Chemical Sensors Applications. *Trends Environ. Anal. Chem.* **2023**, e00204; https://doi.org/10.1016/j.teac.2023.e00204.
128. Fan, J.; Cheng, Y.; Sun, M. Functionalized Gold Nanoparticles: Synthesis, Properties and Biomedical Applications. *Chem. Rec.* **2020**, *20* (12), 1474–1504.
129. Srivastava, N.; Singh, A.; Kumari, P.; Nishad, J.H.; Gautam, V.S.; Yadav, M.; Bharti, R.; Kumar, D.; Kharwar, R.N. Advances in Extraction Technologies: Isolation and Purification of Bioactive Compounds from Biological Materials. In *Natural Bioactive Compounds*; Elsevier: Amsterdam, 2021; pp 409–433.
130. Chen, X.; Xue, Z.; Ji, J.; Wang, D.; Shi, G.; Zhao, L.; Feng, S. Hedysarum Polysaccharides Mediated Green Synthesis of Gold Nanoparticles and Study of its Characteristic, Analytical Merit, Catalytic Activity. *Mater. Res. Bull.* **2021**, *133*, 111070.
131. Asariha, M.; Kiaie, S. H.; Izadi, S.; H. Pirhayati, F.; Fouladi, M.; Gholamhosseinpour, M. Extended-Release of Doxorubicin through Green Surface Modification of Gold Nanoparticles: In Vitro and in Ovo Assessment. *BMC Chem.* **2022**, *16* (1), 110.
132. Khan, M. A.; Singh, D.; Ahmad, A.; Siddique, H. R. Revisiting Inorganic Nanoparticles as Promising Therapeutic Agents: A Paradigm Shift in Oncological Theranostics. *Eur. J. Pharmaceut. Sci.* **2021**, *164*, 105892.
133. Oladipo, A. O.; Lebelo, S. L.; Msagati, T. A. Nanocarrier Design–Function Relationship: The Prodigious Role of Properties in Regulating Biocompatibility for Drug Delivery Applications. *Chem. Biol. Interact.* **2023**, 110466; https://doi.org/10.1016/j.cbi.2023.110466.
134. Abbasi, R.; Shineh, G.; Mobaraki, M.; Doughty, S.; Tayebi, L. Structural Parameters of Nanoparticles Affecting Their Toxicity for Biomedical Applications: A Review. *J. Nanoparticle Res.* **2023**, *25* (3), 43.
135. Gupta, D.; Thakur, A.; Gupta, T. K. Green and Sustainable Synthesis of Nanomaterials: Recent Advancements and Limitations. *Environ. Res.* **2023**, 116316; https://doi.org/10.1016/j.envres.2023.116316.